

Alma Mater Studiorum Università di Bologna
Archivio istituzionale della ricerca

Late Pleistocene to Holocene glacio-eustatic history as recorded in the Pescara paleovalley system (Central Italy, Adriatic basin)

This is the final peer-reviewed author's accepted manuscript (postprint) of the following publication:

Published Version:

Campo B., Barbieri G., Di Martino A., Hong W., Scarponi D., Vaiani S.C., et al. (2022). Late Pleistocene to Holocene glacio-eustatic history as recorded in the Pescara paleovalley system (Central Italy, Adriatic basin). MARINE AND PETROLEUM GEOLOGY, 145, 1-19 [10.1016/j.marpetgeo.2022.105908].

Availability:

This version is available at: <https://hdl.handle.net/11585/900530> since: 2024-05-22

Published:

DOI: <http://doi.org/10.1016/j.marpetgeo.2022.105908>

Terms of use:

Some rights reserved. The terms and conditions for the reuse of this version of the manuscript are specified in the publishing policy. For all terms of use and more information see the publisher's website.

This item was downloaded from IRIS Università di Bologna (<https://cris.unibo.it/>).
When citing, please refer to the published version.

(Article begins on next page)

This is the final peer-reviewed accepted manuscript of:

Campo B.; Barbieri G.; Di Martino A.; Hong W.; Scarponi D.; Vaiani S.C.; Amorosi A.: Late Pleistocene to Holocene glacio-eustatic history as recorded in the Pescara paleovalley system (Central Italy, Adriatic basin). MARINE AND PETROLEUM GEOLOGY 145. ISSN 0264-8172. DOI: 10.1016/j.marpetgeo.2022.105908

The final published version is available online at:

<https://dx.doi.org/10.1016/j.marpetgeo.2022.105908>

Rights / License:

The terms and conditions for the reuse of this version of the manuscript are specified in the publishing policy. For all terms of use and more information see the publisher's website.

This item was downloaded from IRIS Università di Bologna (<https://cris.unibo.it/>)

When citing, please refer to the published version.

Late Pleistocene to Holocene glacio-eustatic history as recorded in the Pescara paleovalley system (Central Italy, Adriatic basin).

Campo B.^{a*}, Barbieri G.^a, Di Martino A.^a, Hong, W.^b, Scarponi D.^a, Vaiani S.C.^a, and Amorosi A.^a

^aDipartimento di Scienze Biologiche, Geologiche ed Ambientali (BiGeA), Università degli Studi di Bologna, Piazza di Porta San Donato 1, 40126, Bologna (Italy). *Corresponding author. E-mail address: bruno.campo@unibo.it.

^bKIGAM Korea Institute of Geoscience and Mineral Resources, 92 Gwahangro, Yuseong-gu, Daejeon Metropolitan City, South Korea

Abstract

A buried paleovalley system, about 50 m deep and 2 km wide, is documented from the Pescara coastal plain. Based on stratigraphic, sedimentological, paleontological, chronological and geotechnical data, the paleovalley profile and 3D facies architecture of the paleovalley fill (PVF) were reconstructed.

The lowermost PVF is a laterally extensive fluvial gravel body, up to 13 m-thick, that represents the lowstand systems tract (LST; pre-11.3 ka cal BP). Above lowstand deposits, the transgressive systems tract (TST), 21 m-thick, shows a deepening-upward trend, from freshwater/inner-estuarine to brackish/outer-estuarine facies associations (11.3-8.0 ka cal BP). The upper part of the succession (highstand systems tract – HST) shows a shallowing-upward tendency from paludal to fluvio-deltaic deposits.

Seven millennial-scale parasequences (Ps) were identified within the Pescara Holocene (TST+HST) succession. Transgressive Ps1-3 exhibit a distinctive retrogradational stacking pattern. Highstand Ps4-7 are aggradationally-to-progradationally stacked. During the aggradational phase (P4), the estuary was gradually filled and swamp environments spread onto the valley interfluvium. Because of subsequent progradation (Ps5-7), delta plain conditions established. In the research core, TST parasequences show higher accumulation rates (up to 9.4 mm/y) than HST ones (1.3-1.8 mm/y). Thus, the study area evolved from a region of sediment storage (11.3-8.0 ka cal BP) into a sector of prevalent sediment bypass (last 8.0 ky).

26 Major early Holocene flooding events were possibly triggered by Melt-Water Pulses (MWP) 1B, 1C
27 and 1D. The eustatic rise linked to MWP-1B reasonably caused the P1 flooding event (11.3 ka cal BP). Post-
28 MWPs 1C and 1D sea-level rises likely provoked the complete drowning of the paleovalley system and the
29 subsequent maximum landward migration of the shoreline (about 8.0 ka cal BP).

30 This study provides new evidences, in terms of sedimentary response, of the poorly-documented MWPs
31 1C and 1D, and the first documentation of MWP-1B eustatic effects in an onshore sector of the Central
32 Adriatic.

33

34 **Keywords**

35 Paleovalley system; facies analysis; millennial-scale parasequences; glacio eustasy; melt water pulses;
36 Adriatic basin

37

38 **1. Introduction**

39 The unquestionable importance of paleovalley systems (PVSs) is signaled by numerous studies that have
40 documented these features in the stratigraphic record. During the last decades, the focus on PVSs was primarily
41 due to their relevance as hydrocarbon reservoirs (Dalla et al., 1997; Dalrymple et al., 1994; Hampson et al.,
42 1999; Harms, 1966; Jennette et al., 1991; Salem et al., 2005) and for the identification of sequence bounding
43 unconformities (Posamentier et al., 1988; Shanley and McCabe, 1994; Van Wagoner et al., 1990, 1988).
44 Following first sequence stratigraphic studies, several authors analyzed ancient (i.e., pre-Quaternary)
45 paleovalley systems to refine concepts and models (Allen and Posamentier, 1993; Legarreta and Uliana, 1998;
46 Shanley and McCabe, 1991; Shanley et al., 1993; Walker, 1995; Wright and Marriott, 1993), and reorganize
47 them into a modern sequence-stratigraphic framework (Catuneanu, 2019, 2006; Catuneanu et al., 2009; Neal
48 and Abreu, 2009; Neal et al., 2016). Paleovalley fills (PVFs) are stratigraphically expanded sedimentary
49 successions that allow preservation of generally poorly-documented stratigraphic intervals (falling-stage and
50 lowstand systems tracts - Blum et al., 1995; Blum and Aslan, 2006; Blum and Price, 1998; Payenberg et al.,
51 2006; Rittenour et al., 2007; Thomas and Anderson, 1994) that can shed new lights on climatic variations in

the past and, especially during glacial/tardiglacial periods (Busschers et al., 2007; Drago et al., 2006; Hanebuth and Stattegger, 2004; Ishiara and Sugai, 2017; Peeters et al., 2015; Simms et al., 2010). In this perspective, Late Quaternary PVSs have been considered as important geological archives and exceptional analogues for the comprehension of ancient systems (Blum and Törnqvist, 2000; Boyd et al., 1989; Kroonenberg et al., 2005; McGhee et al., 2022; Rodriguez et al., 1998; Wang et al., 2020, 2019) and environmental changes driven by allogenic/authogenic forcings (Amorosi et al., 2009; Chaumillon et al., 2010; Durand et al., 2018; Horozal et al., 2021).

More recently, PVSs have been considered as fundamental components of the source-to-sink (S2S) sediment-routing system (Blum et al., 2013). The study of Quaternary PVSs, in particular, may be useful to understand the dynamics of basin-scale sediment transportation pathways from source areas to the deep basin (Sømme et al., 2011; Sweet et al., 2020; Zhang et al., 2021) and to assess reliable sediment budget calculations (Forzoni et al., 2015; Mattheus and Rodriguez, 2014; Phillips et al., 2004). Late Quaternary PVs are also important geological objects in hydrogeological (Barnes et al., 2021; Goetz et al., 2021; Hickin and Best, 2013; Jessen et al., 2008; Seifert et al., 2008; Shaver and Pusc, 1992) and geotechnical (Bishop et al., 2010; Chua et al., 2020; ; Rossi et al., 2011; Truong et al., 2011; Wu et al., 2015; Yanbin and Tongyu, 2016) perspectives. Finally, unconsolidated, post-LGM PVFs have great practical importance, as they can induce significant lateral variations in the effects of ground motions associated with earthquakes (Tanabe et al., 2021, 2015).

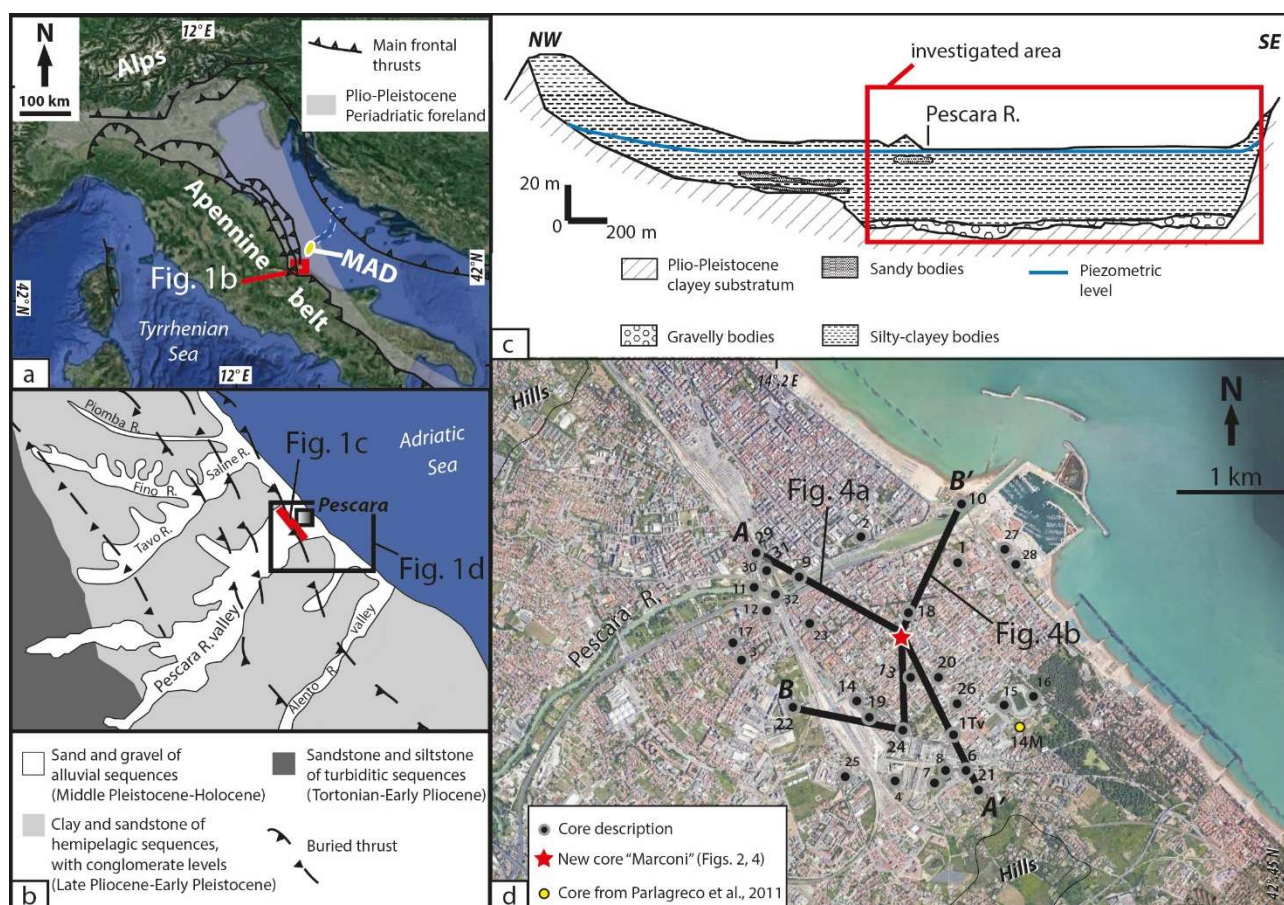
Considering the Po-Adriatic system as an ideal natural laboratory for S2S investigations (Amorosi et al., 2016a), this study aims at the identification of a PVS beneath the Pescara coastal plain (Fig. 1) as a fundamental onshore component of the complex sediment-routing system from the Apennine catchments to the Mid-Adriatic Deep (MAD) basin (Trincardi et al., 1996, 1994; Fig. 1a). In Italy, several PVSs have been documented beneath the Tyrrhenian and Ionian coastal plains (Aguzzi et al., 2007; Amorosi et al., 2013, 2012; Bellotti et al., 2004; Cilumbriello et al., 2010; Grippa et al., 2011; Milli et al., 2016, 2013; Tropeano et al., 2013). In the Adriatic basin, PVSs have been reported from offshore regions, such as the Tavoliere Plain, in Southern Italy (De Santis et al., 2020a, 2020b; De Santis and Caldara, 2016; Maselli et al., 2014; Maselli and Trincardi, 2013), and the Po Delta, in Northern Italy (Ronchi et al., 2018). On the other hand, onshore PSs

78 have only been identified beneath the Venetian-Friulian Plain, in Northern Italy (Ronchi et al., 2021) and the
79 Biferno coastal plain, in Southern Italy (Amorosi et al., 2016b).

80 Thus, a documentation gap exists for the Central Adriatic, characterized by a 50 km and 0.2° dip shelf
81 descending directly into the small MAD basin (Maselli et al., 2011). Whereas the stratigraphic setting of this
82 offshore basin is already well-known (Cattaneo et al., 2007; Correggiari et al., 1996; Gamberi et al., 2020;
83 Pellegrini et al., 2021, 2018; Piva et al., 2008a, 2008b), the stratigraphy of coeval successions onshore is almost
84 unexplored in this sector of the Central Adriatic. This work aims at filling this gap documenting the first Late
85 Pleistocene-Holocene coastal plain paleovalley in front of the MAD, as the preliminary study for future and
86 ongoing basin-scale S2S investigations with important implications for refining and improving hydrocarbon
87 exploration models (Bhattacharya et al., 2016; Leithold et al., 2016; Liu et al., 2019; Zeng et al., 2019).

88 The occurrence of a late Quaternary PVS beneath the city of Pescara was suggested by Desiderio et al.
89 (2007) in a preliminary hydrostratigraphic study on the basis of basic lithological descriptions. This study
90 showed that the Plio-Pleistocene marine substrate (Fig. 1c) is unconformably overlain by Holocene alluvial
91 deposits (up to 50 m thick), with a lower, < 10 m thick gravel body overlain by a thicker fine-grained interval
92 with isolated sand bodies (Fig. 1c). More recently, Parlagreco et al. (2011) analyzed the uppermost 19 m of a
93 distal sector of the Pescara coastal plain. They dated a brackish/lagoonal interval (ca. 13-9.4 m core depth) to
94 about 7.7-6.8 ka cal BP, and uppermost coastal/continental sands to the last 4.0 ky. No other scientific studies
95 are available from this area. As a result, the stratigraphic architecture of the Pescara PVF and general
96 paleoenvironmental evolution of the study during the last 30 ky are poorly known. Our investigation mostly
97 focused on the paleovalley depocenter, south to the modern Pescara River axis (Fig. 1c, d), with the aim of
98 exploring all stratigraphic components of the valley fill.

99 The main objectives of this work are: to achieve the high-resolution (millennial-scale) stratigraphic
100 analysis of the Pescara valley fill; to reconstruct the three-dimensional (along-dip and along-shore) facies
101 architecture; to accomplish the sequence stratigraphic interpretation of the investigated succession; to evaluate
102 the glacio-eustatic control on facies architecture and sediment accumulation during the last 30 ky.



2. Geological and geomorphological setting

The Pescara coastal Plain represents the distal sector of the Pescara River valley (Fig. 1). The latter, several kilometers in width (D'Alessandro et al., 2001), is drained by the Pescara River (45 km long), which is fed by the Aterno and Sagittario tributaries. As a whole, the hydrographic basin is about 3170 km² (Urbano

117 et al., 2017). The average sediment discharge of the Pescara River is about 1,500 kT/yr (Syvitski and Kettner,
118 2007).

119 The Pescara coastal plain is located along the Central Adriatic coast, between the Apennine thrust belt
120 and the Periadriatic foreland (Fig. 1a). An eastward-dipping regional monocline characterizes the structural
121 setting (Ascione et al., 2008; D'Alessandro et al., 2008). Fold and fault systems, buried underneath sedimentary
122 strata, mainly show SW-NE direction (Fig. 1b) and alluvial valleys display similar orientation (Desiderio et
123 al., 2007). Beneath the Pescara coastal plain, the main fault systems consist of buried thrusts (Della Seta et al.,
124 2008).

125 The study area and the adjacent coastal plain experienced generalized tectonic uplift during the Middle
126 Pleistocene (Bracone et al., 2012a), and then remained stable up to the Holocene (Antonioli et al., 2009;
127 D'Amico et al., 2013). Based on sedimentological, paleontological and chronological data from a
128 continuously-cored borehole retrieved in the study area (Fig. 1 for location) and the identification of five "sea-
129 level markers", after paleo-sea level corrections and correlations with additional stratigraphic and
130 morphotectonic data, Parlagreco et al. (2011) concluded that during the last 7,000 years, along the lower trunk
131 of the Pescara valley, vertical tectonic displacements were negligible. Seawards, subsidence rate is about
132 0.3 mm/y in the Central Adriatic, the (Maselli et al., 2010).

133 The piedmont reliefs are characterized by the Plio-Pleistocene syn-orogenic marine succession (Ori et
134 al., 1991; Bigi et al., 1995; D'Alessandro et al., 2003), which is made of siliciclastic clay, sands and
135 conglomerates (Fig. 1b). These marine deposits mostly belong to the Mutignano Formation (Crescenti and
136 D'amato, 1980). This unit crops out at the Apennine foothills between the valleys (Fig. 1b) as a wide homocline
137 that gently dips north-east (Urbano et al., 2017), and that consists of offshore to shoreface facies associations
138 (Ori et al., 1986; Geological Map of Italy at 1:50,000 scale, Sheet 351). The Plio-Pleistocene succession
139 unconformably overlies the Messinian-Early Pleistocene turbidites of the Periadriatic foredeep (Della Seta et
140 al., 2008) and typically includes the upper part of the Argille Azzurre Formation (Bracone et al., 2012b).
141 Beneath the Pescara River, the thickness of the Plio-Pleistocene succession ranges between 2,000 m and 500
142 m in the main depocenters and atop structural highs, respectively (Desiderio et al., 2007). This sequence is
143 overlain with a Middle Pleistocene-Holocene continental succession composed of alluvial, transitional to

144 coastal deposits (D'Alessandro et al., 2003). Four orders of alluvial terraces (Middle-Late Pleistocene), mostly
145 made up of gravel and sand bodies, have been recognized on the W-NW flank of the Pescara valley (Parlagreco
146 et al., 2011; Geological Map of Italy at 1:50,000 scale, Sheet 351). The origin of these terraces has been related
147 to the interaction between Quaternary tectonics and high-frequency glacio-eustatic and climatic variations
148 (Della Seta et al., 2008). In the proximity of the Pescara River mouth (Fig. 1b), the alluvial valley fill of
149 Holocene age consists of a 10 m-thick gravel body capped by 50 m thick silty-clay sediments (Fig. 1c;
150 Desiderio et al., 2007).

151 Offshore, the Adriatic continental shelf reaches the Mid-Adriatic Deep (MAD; Fig. 1a). While the shelf
152 is characterized by sandy-silty depositional sequences (Ridente et al., 2008; Trincardi et al., 1994) the MAD
153 is a small slope basin, up to 260 m deep, where fine-grained sediments accumulated almost continuously during
154 the last 370 ky (Piva et al., 2008a, b). The MAD was progressively filled by Po River sediments during several
155 Quaternary phases of sea-level fall and lowstand (Dalla Valle et al., 2013a, b). The stepwise sea-level lowering
156 that followed the Last Interglacial (Marine Isotope Stage 5e or MIS 5e, ca., 130 ka cal BP) caused a marked
157 basinward shift of the shoreline, the formation of an unconformity of regional extent, and alluvial plain
158 sedimentation took place in the northern Adriatic shelf (Amorosi et al., 2016a). At the end of the Last Glacial
159 Maximum (MIS 2), the MAD was partially filled with the Po River Lowstand Wedge (Pellegrini et al., 2018).
160 This lowstand delta prograded 40 km throughout the shelf edge forming a 350 m-thick complex sedimentary
161 body between 30-14 ka cal BP (Pellegrini et al., 2017).

162

163 **3. Methods**

164 **3.1 Facies analysis**

165 The three-dimensional stratigraphic architecture of the Pescara coastal plain succession (Late
166 Pleistocene-Holocene) was reconstructed across two transects with NW-SE and SW-NE orientation,
167 respectively, each about two kilometers long (Fig. 1d). Stratigraphic correlation was carried out based on
168 geometric criteria constrained by radiocarbon ages. The dataset consists of 32 borehole descriptions (average
169 depth ca. 45 m) available from the “Microzonazione Sismica Project” of the Pescara Municipality.

170 Facies interpretation was based on integrated sedimentological and paleontological (benthic foraminifer,
171 ostracod and mollusk) analyses that were carried out on the 52 m-long reference core “Marconi” (Fig. 1d).
172 This core was specifically acquired as part of the study from the Pescara coastal plain, about 1 km landward
173 of the modern shoreline, at 1.35 m asl. Core Marconi was described in terms of texture, mean grain-size, color,
174 sedimentary structures, and accessory materials, such as wood fragments, plant remains, fossil content and
175 carbonate concretions (Fig. 2). Pocket penetration (compressive strength) values from fine-grained deposits
176 (Fig. 2) were also considered for facies interpretation following the criteria outlined by (Amorosi et al., 2015).
177 For stratigraphic correlation in a predominantly freshwater environment, we used the techniques adopted from
178 recent work in the Po coastal plain. In particular, it expands the parasequence concept (Van Wagoner et al.,
179 1990, 1988) to the paralic/estuarine realm, where paludification surfaces at the base of peats may delineate the
180 updip (freshwater) equivalents of brackish/marine flooding surfaces more readily identified at seaward
181 locations (Amorosi et al., 2021) due to sharp (marine to brackish) facies changes.

182 A total of 79 and 50 samples (Fig. 2) were collected for meiofauna (ostracods and foraminifers) and
183 malacofauna analyses, respectively. These data allowed to retrieve palaeoenvironmental information about
184 organic matter concentration, paleosalinity, paleobathymetry and substrate characteristics. For
185 micropalaeontological analyses, samples (100-150 g) were treated according to standard procedures previously
186 adopted in other works on late Quaternary successions (e.g., Barbieri et al., 2021; Rossi and Vaiani, 2008).
187 Samples were dried at 60 °C, soaked in 10% H₂O₂, water-screened with a 63 µm sieve, dried again and dry-
188 sieved at 125 µm.

189 Samples (400-700 g, depending on lithology) for mollusk-based inferences were collected at selected
190 stratigraphic positions along the stratigraphic succession (Fig. 2). Based on (Azzarone et al., 2020), samples
191 were dried at 40°C, soaked in hydrogen peroxide solution 4% and wet sieved at 1 mm screens. The resulting
192 material was qualitatively analyzed under an optical microscope to describe fossil assemblages. For each
193 sample macrobenthic remains were speditively counted as rare ($n \leq 10$) or common ($n > 10$ fossils, respectively)
194 and identified, whenever possible, to species level.

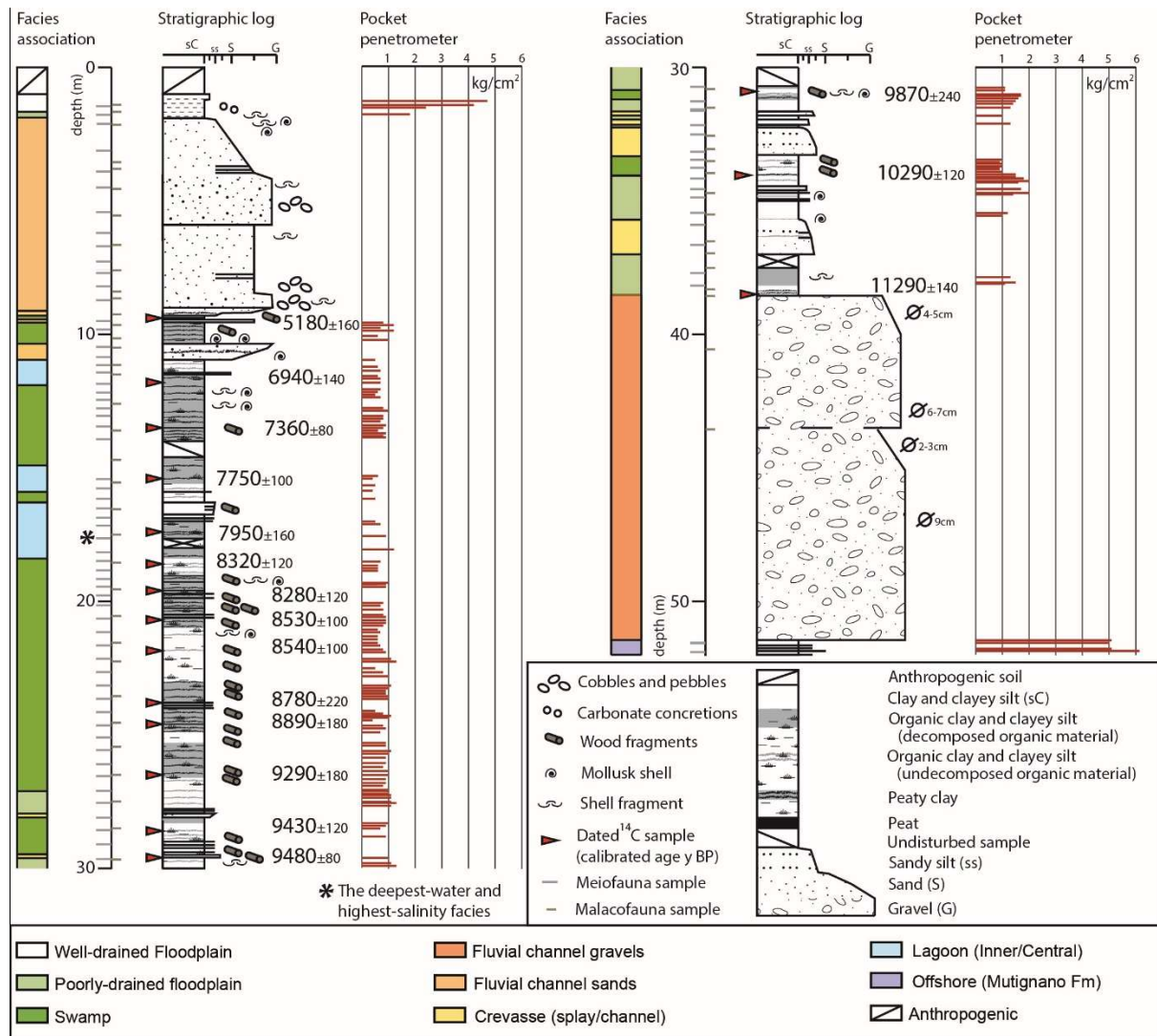


Fig. 2 – Facies interpretation and pocket penetration values of reference core Marconi (see Fig. 1d for location).

The identification of meiofaunal taxa was supported by original descriptions (Ellis and Messina, 1940, 1952), integrated with selected papers (Athersuch et al., 1989; Barbieri and Vaiani, 2018; Henderson, 1990). Autoecological characteristics and modern distribution of ostracods and foraminifers derive mainly from Coccioni (2000), Debenay et al. (2000), Meisch (2000), Milker and Schmiedl (2012), and Pint and Frenzel (2017). Mollusk identification relied on the late Quaternary fossil collections of the Stratigraphic Paleoecology Laboratory of the Department of Biological, Geological and Environmental Sciences, University of Bologna.

3.2 Chronology

206 The high-resolution chronological framework rests on seventeen AMS ^{14}C dates (Fig. 2 and Table 1)
 207 performed on organic-rich samples (wood fragments and charcoals) at KIGAM Laboratory (Daejeon, Republic
 208 of Korea), after acid-alkali-acid pretreatment. All samples were previously cleaned with deionized water and
 209 dried at 40° C to prevent mold formation. Conventional ^{14}C ages were calibrated using OxCal 4.4 (Ramsey,
 210 1995; Ramsey and Lee, 2013) with the IntCal 20 and Marine 20 curves (Reimer et al., 2020). Five dates on
 211 shells from Parlagreco et al. (2011) were recalibrated following facies attribution (brackish/lagoon vs marine)
 212 and the suggested correction of 487 ± 29 y for the Central Adriatic Sea (Table 1).

213 The reliability of the 17 new radiocarbon dates (Fig. 2; Table 1) was tested by using the Bayesian
 214 approach (Blockley et al., 2004), which allows incorporating prior information into the calibration process
 215 (Buck et al., 2003, 1992, 1991). In particular, the form of Markov Chain Monte Carlo (MCMC) analysis
 216 available in OxCal has been utilized. An age-depth model (Lowe et al., 2007; see Supplementary materials)
 217 was developed to eventually reject dates of poor fit and constrain the whole series objectively. The *General*
 218 *setting* was adopted for the Outlier-Model analysis, and the prior probability fixed to 0.05. Similar Bayesian
 219 methodology was used by Tesi et al. (2017) for the investigation of coeval (Holocene) offshore-deep marine
 220 deposits in the Central and Southern Adriatic.

221

222 *Table 1 – List of radiocarbon dated samples from reference core Marconi and ^{14}C dates* (AMS) from*
 223 *Parlagreco et al. (2011; recalibrated) shown in Figs. 2, 3 and 4.*

Lab Nr.	Material	Core Depth (m)	C14 age (BP)	Cal year BP (2 σ range)	C14 age (2 σ) Cal BP (mean error)	Figure
KGM-OWd210391	wood fragments	9.4	4535 ± 33	5200-5050	5180 ± 160	2, 3, 4
KGM-OWd210392	wood fragments	11.8	6079 ± 37	7030-6790	6940 ± 160	2, 4
KGM-OWd210393	wood fragments	13.5	6444 ± 37	7430-7270	7360 ± 80	2
KGM-OWd210394	wood fragments	15.4	6919 ± 41	7850-7660	7750 ± 100	2, 4
KGM-OWd210396	wood fragments	17.4	7134 ± 39	8020-7920	7950 ± 160	2, 3, 4
KGM-OWd210397	wood fragments	18.6	7522 ± 40	8410-8280	8320 ± 120	2, 3, 4
KGM-OWd210398	wood fragments	19.6	7473 ± 44	8370-8190	8280 ± 120	2

KGM-OWd210399	wood fragments	20.7	7766 ± 42	8610-8420	8530 ± 100	2
KGM-OWd210400	wood fragments	21.85	7778 ± 43	8640-8430	8540 ± 100	2
KGM-OWd210401	wood fragments	23.8	7925 ± 40	8990-8600	8780 ± 220	2
KGM-OWd210402	wood fragments	24.6	8035 ± 43	9030-8720	8890 ± 180	2
KGM-OWd210403	wood	26.5	8288 ± 44	9440-9120	9290 ± 180	2, 4
KGM-OWd210404	wood	28.6	8405 ± 40	9530-9390	9430 ± 120	2, 4
KGM-OWd210405	wood fragments	29.6	8458 ± 47	9540-9410	9480 ± 80	2
KGM-OWd210406	wood fragments	30.9	8812 ± 39	9970-9680	9870 ± 240	2, 4
KGM-OWd210407	wood fragments	34.05	9123 ± 43	10410-10200	10290 ± 120	2, 4
KGM-OWd210408	charcoal	38.5	9874 ± 48	11410-11190	11290 ± 140	2, 3, 4
6009*	Marine shell	3.0	2880 ± 30	2040-1680	1850 ± 180	4
6010*	Marine shell	6.4	4125 ± 35	3550-3200	3380 ± 180	4
6011*	Lagoon shell	8.4	6400 ± 40	6850-6570	6710 ± 120	4
6012*	Lagoon shell	9.0	6870 ± 40	7410-7160	7260 ± 120	4
6013*	Brackish shell	11.0	6860 ± 40	7410-7150	7250 ± 120	4

4. Substrate and Facies associations

Based on the integrated sedimentological and paleontological analysis of core “Marconi”, seven facies associations were identified (Fig. 2) above the Mutignano Formation substrate. Substrate and facies associations are described in detail below in stratigraphic order. Their interpretation is based on sedimentological features, fossil (meiofauna and mollusk) content, stratigraphic relationships, and geotechnical properties (pocket penetration measurements).

4.1 Mutignano Formation (Mt Fm) substrate

Description. This sedimentary unit consists of gray to brownish clays and silty clays with cm-thick sand intercalations (Fig. 3). Horizontal lamination is common. Bioturbation is locally present. This sedimentary unit was encountered in the lowermost part of the reference core, up to about 51.5 m core depth (Figs. 2-3). It is characterized by very high pocket penetration (Pp) values, invariably > 5 kg/cm² (Fig. 2).

Fig. 3 – Representative photographs of the incised substrate and facies associations identified in core Marconi. Silty clays with cm-thick sand intercalations of the marine substrate (Mutignano Formation – Mt Fm). Fluvial-channel gravels (FCg) with calcareous rounded pebbles and cobbles, showing erosional lower base (red line) and fining-upward (FU) tendency. Massive, gray to darkish poorly-drained floodplain (PDF) silty clays. Swamp (Sw) dark gray to blackish clays with very high organic matter content, abundant vegetal/wood remains and peat layers. Silty sands with FU trend and erosional base of crevasse-channel (CrC) deposit. Coarsening-upward (CU) tendency within crevasse splay (CrS) sediments. Lagoonal (Lg) gray to darkish clays and silt clays with abundant wood fragments, bioclasts and decomposed organic content. Unrecovered (Ur) core interval. Fluvial-channel sands (FCs) with FU trend and erosional lower base. Mottled well-drained floodplain (WDFP) gray to brownish clays and silty clays. Anthropogenic (An) deposit. Calibrated ages (a BP; white color).

4.2 Facies associations

4.2.1. Fluvial-channel (gravel - FCg) facies association

Description. This facies association, up to 13 m thick, includes amalgamated and poorly sorted gravel deposits with calcareous rounded pebbles and cobbles (ranging from 2 to 9 cm in diameter) locally embedded in a silty-sandy whitish matrix (Fig. 3). An erosional lower boundary cutting into the marine substrate characterizes this composite facies association, made of two vertically-amalgamated gravel bodies with peculiar fining-upward trends (Figs. 2 and 3). Microfossils are absent. Neither mollusk shells nor wood fragments were encountered. For this facies association, radiocarbon ages are not available.

Interpretation. The very coarse texture, internal FU trends and the erosional lower boundary are characteristic of high-energy and high-gradient fluvial-channel (FC) deposits (Miall, 1992). Poor sorting, presence of cobbles and pebbles along with amalgamation surfaces are consistent with a braided stream facies that accumulated in a confined and very high-energy flow setting, probably characterized by high topographic gradient and morphological confinement, within the narrow, piedmont Pescara valley (Fig. 1). The lack of fossils and of vegetal remains is consistent with this interpretation.

4.2.2 Channel-related (CrS-CrC) facies association

Description. This facies association consists of two different lithofacies: silty sand deposits with maximum thickness of 1.3 meters with FU trend, erosional base and gradational top (Fig. 3); and sandy silt to coarse sand bodies, a few decimeters thick, displaying general coarsening-upward (CU) tendency with gradational lower boundary and sharp top (Fig. 3). Silty intercalations are locally encountered, along with scarce wood and shell fragments. Samples retrieved for palaeontological analyses are barren or include few freshwater mollusk remains (*Pisidium* sp. and *Bithynia* opercula).

Interpretation. Sedimentological and paleontological characteristics suggest a variety of sub-environments dominated by fluvial processes, close to the river axis. The presence of vegetal remains and fragments of freshwater bivalves (e.g., *Pisidium*) or gastropods opercula (e.g., *Bithynia*) is consistent with overbank sub-environments exposed to frequent river floods. Thin sand bodies with CU tendency and gradational base are interpreted to be crevasse splays (CrS). Fining-upward sandy deposits, less than 1.5 m thick, with erosional lower boundary are supposed to represent crevasse channels (CrC).

4.2.3 Poorly-drained floodplain (PDF) facies association

Description. This facies association, generally less than 1.5 m thick (Fig. 2), is made up of massive gray to darkish gray clay and silty clay (Fig. 3). Pedogenic features are absent. Thin layers of decomposed organic material, a few cm-thick, are common, whereas wood and charcoal debris are scattered (Fig. 3). Silty sand intercalations, a few mm to cm-thick, are scattered within this facies association, which occurs at various stratigraphic levels in the reference core between 27 and 35 m core depth (Fig. 2). Radiocarbon dates available for this interval indicate an age ranging between 11.3 and 9.2 ka BP. Pocket penetration measurements fall in the interval of 1.0-1.7 kg/cm² (Fig. 2). Ostracod assemblages consist of low amounts of freshwater species, such as *Candona neglecta*, *Ilyocypris* spp. and *Pseudocandona albicans*. The macrobenthic content is represented by sparse fragments of freshwater and terrestrial gastropods, though mollusk shells are locally present (i.e., 38.4 m and 27.5 m core depth; Figs. 2 and 3). The lowermost fossil-rich horizon is dominated by the calciphile and pulmonate gastropod *Pomatias elegans* (common). Whereas the uppermost one is characterized by *Bithynia* opercula (common) and *Valvata* sp. specimens (common).

302 Interpretation. The fine-grained lithology, absence of pedogenic features and oxidation combined with
303 the occurrence of a freshwater fauna (*Candona neglecta*, *Ilyocypris* spp. and *Pseudocandona albicans*) and
304 shell fragments (from *Pomatias elegans* to *Bithynia* and *Valvata* remains) are consistent with deposition in a
305 low-energy environment, most likely characterized by low topography, frequent river floods and generally
306 high-water table or ephemeral standing bodies of freshwater typical of poorly-drained floodplain settings. The
307 microbenthic content at 38.4 m and 27.5 m depth reflects locally increasing water table. Pocket penetrometer
308 data support this interpretation, suggesting a depositional setting with high water content that produced
309 relatively low soil consistency, transitional between well-drained floodplain and paludal deposits.

310 4.2.4 Swamp (Sw) facies association

311 Description. This facies association, up to 9 m thick in the reference core (Fig. 2), is composed of very
312 soft dark gray to blackish clays (Fig. 3). Organic matter content is very high, including abundant millimetric
313 to centimetric-sized plant debris and wood fragments (Fig. 3). Peat layers (less than 15 cm-thick) occur at
314 different stratigraphic intervals. Silt and silty sand intercalations, a few centimeters thick are also present. A
315 rich ostracod fauna is commonly found within this facies association: it is dominated by the same species found
316 in PDF sediments, with the local occurrence of other subordinate taxa, such as *Cypria ophtalmica*,
317 *Fabaeformiscandona* sp. and *Cyclocypris* sp. In the upper part of the unit, rare specimens of euryhaline
318 ostracods (*Cyprideis torosa*) and benthic foraminifers (*Ammonia tepida*) are observed in association with
319 dominant freshwater to mesohaline ostracods. Mollusk shell fragments are abundant. A relatively rich
320 macrobenthic assemblage was observed at 29.7 m and 12.6 m core depth, respectively (Fig. 2). This fossil
321 assemblage includes a suite of freshwater-to-oligohaline taxa, such as *Planorbis* spp. (common), *Valvata* sp.
322 (common), *Pisidium* spp. (rare), *Succinea* sp. (rare), *Theodoxus fluviatilis* (rare) and hydrobiids.

323 Pocket penetrometer measurements are generally lower than 1 kg/cm² with slightly higher values (up to
324 1.2 kg/cm²) recorded into peaty intervals (Fig. 2). This facies association commonly overlies poorly-drained
325 floodplain deposits and is dominant between 18-30 m core depth (Fig. 2). Radiocarbon dates from this facies
326 association suggest an age ranging between 9.4-8.3 ka BP (Fig. 2, Table 1). Between 16.3 and 9.4 m core
327 depth, this facies association is sandwiched between lagoonal and fluvial deposits. Two ages of 7.3 and 5.2 ka
328 cal BP are available for this interval (Figs. 2, 3 and Table 1).

329 Interpretation. Lithological characteristics, very-high amounts of organic matter, the presence of peat
330 and very low Pp values are coherent with a low-energy environment, such as a wetland. Lack of traces of
331 oxidation, rare coarser beds and abundant organic matter content are consistent with waterlogging and reducing
332 conditions typical of a paludal environment, away from an active channel (Bruno et al., 2019). The rare
333 occurrence of euryhaline taxa suggests the local onset of mesohaline conditions. Freshwater to low-brackish
334 conditions are typical of swamps in the inner sector of an estuary.

335 4.2.5 Well-drained floodplain (WDFP) facies association

336 Description. This facies association is encountered only in the topmost 2 m of the reference core (Figs.
337 2-3), but also at different stratigraphic levels in cores 9 and 6 (see Fig. 1 for location), between 34-37 m bsl. It
338 is less than 1 m thick, and consists of rooted, pedogenized gray to brownish clay and silty clay with yellowish
339 mottles due to manganese and iron oxides. Silty sand intercalations and carbonate nodules can be present. The
340 meiofauna is absent. Shell-rich horizons dominated by the continental mollusk *Cerneuella* and few
341 reworked/transported shells of shoreface bivalves are locally observed (e.g., 1.7 m core depth Fig. 2). Based
342 on the sedimentological data from available core descriptions and stratigraphic correlations, this facies
343 association displays a remarkable lateral continuity extent in the uppermost interval of the succession. Pocket
344 penetration values range between 2.4 and 4.7 kg/cm² (Fig. 2).

345 Interpretation. Lithology, pedogenic features and geotechnical characteristics allow interpreting this
346 facies association as accumulated in a well-drained floodplain. Fine-grained lithologies, presence of roots and
347 pedogenized horizons are consistent with a low-energy depositional environment typified by subaerial
348 exposure under well-drained conditions, due to a very low water table position. The presence of land mollusks
349 characteristic of dry coastal plain settings and open habitats, such as *Cerneuella* (Grano and Di Giuseppe, 2021),
350 along with the lack of meiofauna, also support this interpretation.

351 4.2.6 Lagoon (Lg) facies association

352 Description. This facies association, up to 2 m thick in the reference core (Fig. 2), consists mostly of
353 very soft gray to darkish clays. Silt clays with sandy silt and silty sand intercalations showing a CU trend are
354 also encountered (10.35-10.90 m core depth, Fig. 3). Wood fragments and vegetal remains are abundant (Fig.

355 3). Decomposed organic matter is also diffused, and millimetric-sized shell fragments are locally widespread
356 (Fig. 3). This facies association shows vertical transition to paludal clays, within 11-18 m core depth (Fig. 2).
357 The lower and upper parts of this facies association were radiocarbon dated to about 8.0 and 7.0 ka cal BP,
358 respectively (Fig. 2). The meiofauna consists of abundant euryhaline ostracods (*Cyprideis torosa*) and
359 foraminifers (*Ammonia tepida* and rare *Ammonia parkinsoniana* and *Haynesina germanica*). A more
360 diversified assemblage, including other brackish to euhaline ostracods and foraminifers, such as *Loxoconcha*
361 *elliptica*, *Xestoleberis aurantia* and *Criboelphidium oceanensis*, was found between 17 and 18 m core depth.
362 As for mollusk remains, most samples yielded only few brackish specimens. Two mollusk-rich assemblages
363 were retrieved at 17.5 m and 11.20 m core depth (Fig. 2). The lower assemblage is dominated by the brackish
364 to marine gastropods *Bittium reticulatum* and *Rissoa* spp. (both common), the brackish minute gastropod
365 *Ecrobia* cf. *ventrosa* (common) along with few freshwater specimens of *Valvata* sp.. Whereas the upper
366 mollusk association is characterized by *Ecrobia* cf. *ventrosa* (common) along with *Abra segmentum* (rare) and
367 thin-shelled *Cerastoderma* spp. (rare). Pocket penetration values are very low, ranging between 0.4-0.9 kg/cm²
368 (Fig. 2).

369 Interpretation. Sedimentological characteristics and fossil assemblages suggest a low-energy, lagoonal
370 (or outer-estuary) depositional environment, typified by generally abundant organic content, and brackish
371 conditions. Fossils in the lower part of this unit (between 18 and 17 m core depth) reveal a relatively high
372 marine influence, consistent with a central lagoon environment, as indicated by i) a diversified, brackish and
373 euryhaline meiofauna, and ii) mollusk taxa adapted to live in mesohaline to fully marine salinity settings (e.g.,
374 *B. reticulatum*), along with rare freshwater species. In contrast, in the upper part of this facies association, the
375 meiofauna and mollusks are considered to reflect inner lagoon conditions with a low marine influence, as
376 suggested by i) few species of ostracods and foraminifers and ii) the common presence of hydrobids, thin-
377 shelled *Cerastoderma* and *A. segmentum*, taxa preferentially distributed in mesohaline to oligohaline settings
378 elsewhere along the Adriatic and beyond (e.g., Amorosi et al., 2014; Scarponi et al., 2017).

379 4.2.7 Fluvial/distributary-channel (sand - FCs) facies association

380 Description. This facies association was identified in the uppermost 10 m of the reference core, above
381 paludal deposits. Poorly-drained floodplain clays cap this facies association, which generally consists of sand

bodies (about 7 m thick) with erosional lower base and FU trend: from basal gravelly-coarse to medium gray sands with rounded pebbles to silty sands (Fig. 3). Internal erosional boundaries can also be observed (Fig. 2). Silty and silty clay cm-thick intervals are locally encountered, along with a few shell fragments of shoreface bivalves. This facies association is generally barren of microfossils. In cores 9, 6 and 22 (Fig. 1 for location), this unit is sandwiched between swamp clays and shows a slight upward decrease in grain-size, with the dominance of silty sands and sandy silts.

Interpretation. Lithology, grain-size tendency, and erosional lower base allow the interpretation of this facies association as a sandy fluvial-channel deposit (Bridge, 2006). The local abundance of rounded pebbles supports this interpretation. As regards sand deposits in cores 9 and 6, the vertical transition to paludal clays coupled with finer grain size suggest their interpretation as a distributary-channel deposit (Bhattacharya, 2006). As for the mollusk content, the local presence of shoreface shell fragments is considered to reflect exceptional on land transport and might point to a portion of the fluvial network adjacent to (or interfingering with) backshore settings, in a wave-dominated deltaic environment.

4.2.8 *Beach-ridges/Delta-front/Transgressive barrier facies association*

Description. This facies association was not penetrated by core Marconi. It crops out in the easternmost sector of the studied succession, in proximity of the modern shoreline, as reported by the stratigraphic description of core 10 (Fig. 1 for location). This facies association, up to 22 m thick, is composed of medium to fine sands with frequent pebble (rounded) intercalations, gradational lower boundary with underlying organic-rich clays and an overall CU trend. Bioclasts accumulation is a common feature of this deposit.

Interpretation. Lithology, sedimentological features and the distal position are consistent with a high-energy marine (coastal) setting for this outcropping sand body. Presence of scattered bioclasts alternating with rounded pebbles may suggest a marine environment highly influenced by fluvial activity, such as a delta-front setting. Based on the chronology available from the reference core (Fig. 2; Table 1), stratigraphic correlations suggested that this facies association started to accumulate above estuarine deposits in response to the Middle Holocene transgression, around 8.3 ka cal BP. The maximum thickness is linked to Middle-Late Holocene delta progradation (last 7.8 ky).

4.2.9 *Anthropogenic facies association*

Description. This facies association, up to 2.5 m thick, was identified between 0-1 m depth in the reference core (Fig. 2). It is characterized by chaotic, unconsolidated and unsorted deposits of different provenance (Fig. 3). The coexistence of materials of both natural (sediment, wood) and human (bricks, plastic and iron fragments) origin is peculiar of this deposit which was identified in several core descriptions (22, 1, 29, 31, 9, 13, 20, 2, 1Tv, 6 and 21) at the core surface. Widespread blocks and cobbles generally have undifferentiated origin and show angular, sub-angular or rounded shapes (Fig. 3). No sedimentary structures were observed.

Interpretation. Stratigraphic positions, lack of sedimentary structures and the presence of clearly man-made materials such as plastic fragments, allow the attribution of this facies association to human activity. In particular, the unsorted and unconsolidated deposits are associated to landfill activities, whereas levels of sub-angular clasts may reflect building foundations.

5. Paleovalley fill architecture and sequence-stratigraphic interpretation

5.1 Stratigraphic architecture

Two stratigraphic panels, one transverse (Fig. 4a) and the other one parallel (Fig. 4b) to the valley axis (Fig. 1d for location), depict the stratigraphic architecture of the paleovalley fill. Their orientation allowed a basic three-dimensional reconstruction of the paleovalley profile and of facies relationships.

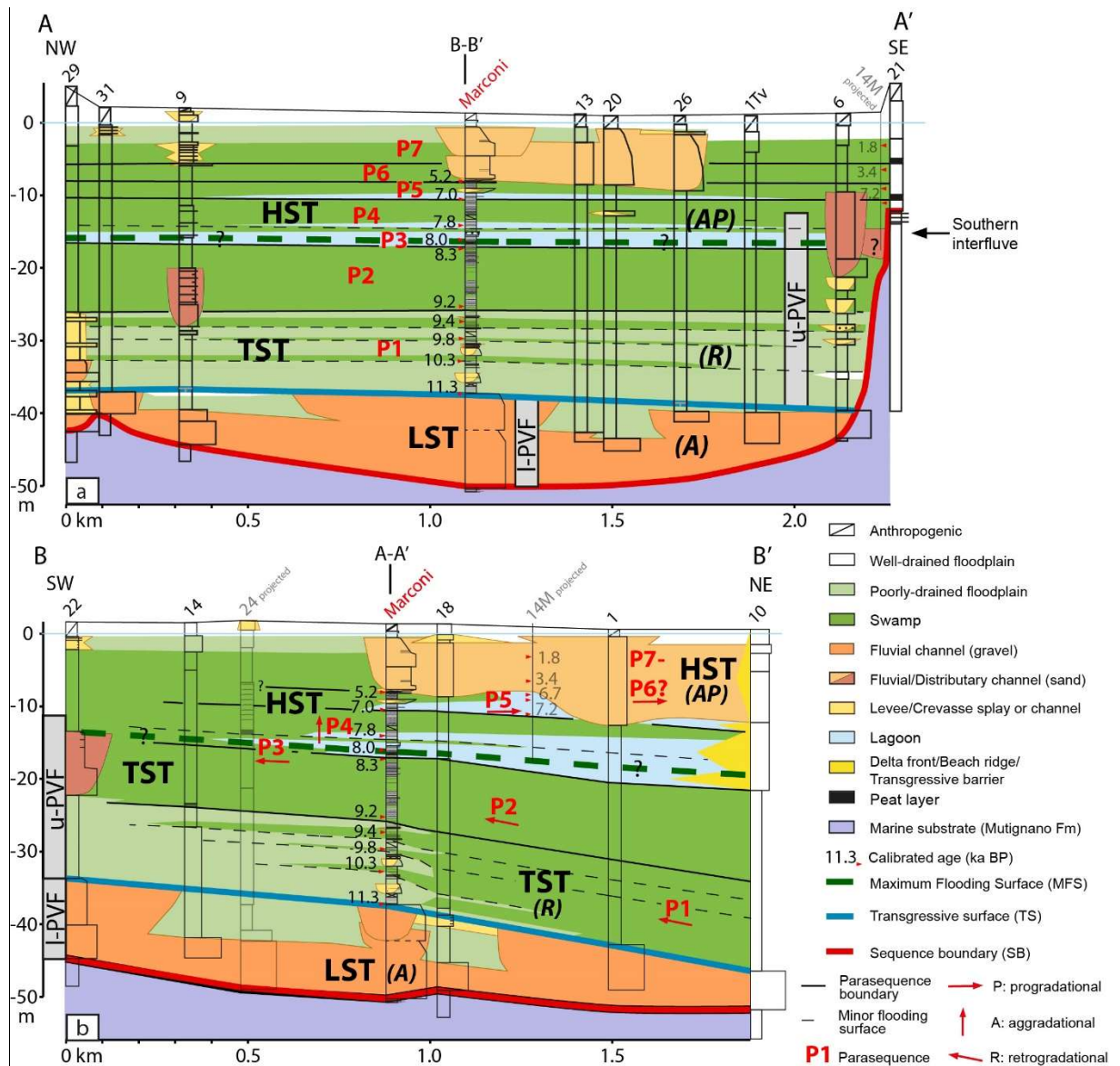


Fig. 4 – Stratigraphic panels illustrating the transversal (a) and longitudinal (b) facies architecture beneath the Pescara coastal plain (see Fig. 1 for section traces) with indication of lower (l-PVF) and upper (u-PVF) paleovalley fills; and sequence stratigraphic interpretation (LST: lowstand systems tract; TST: transgressive systems tract; HST: highstand systems tract). Seven parasequences are numbered in red. Reference core is also indicated in red.

Beneath the Pescara valley, the paleovalley profile and valley fill were identified and tracked from the depocenter (core “Marconi”) to the southern interfluvium (core 21; Fig. 4a) on the basis of the abrupt facies change between Early Pleistocene marine silty clays of the Mutignano Fm and continental deposits of Late

437 Pleistocene-Holocene age (Fig. 4a, b). On the valley floor, between about 40-50 m depth (Fig. 4a, b), offshore
438 deposits of the Mutignano Fm are overlain by laterally extensive, amalgamated fluvial gravel bodies (Fig. 4a,
439 b). Southwards, at about 12 m depth (core 21, Fig. 4a), soft (mean $P_p < 1.0 \text{ kg/cm}^2$) organic-rich Holocene
440 deposits overlie the stiff (mean $P_p > 5 \text{ kg/cm}^2$) substrate. Overall, the Pescara paleovalley is about 50 m deep
441 and, at least, 2 km wide (Fig. 4a), possibly up to 3.5 km considering the unsurveyed northern sector shown in
442 Fig. 1c.

443 The Pescara paleovalley fill is similar to many ancient and Late Quaternary PVFs (Allen and
444 Posamentier, 1993; Aslan and Blum, 1999; Blum and Womack, 2009; Boyd et al., 2006; Busschers et al.,
445 2007, 2005; Cross et al., 1993; Dalrymple et al., 2006; Gibling and Bird, 1994; Guijia and Congxian, 1996;
446 Hori et al., 2002; Plint and Nummedal 2000; Shanley and McCabe, 1994, 1991; Tanabe et al., 2006; Van
447 Wagoner, 1995; Zaitlin et al., 1994) in terms of facies architecture and fluvial stacking patterns: a laterally
448 extensive fluvial body (i.e., the lower paleovalley fill or l-PVF; Fig. 4) with erosional base and upward
449 transition to more isolated sand bodies within a mud-dominated succession (the upper paleovalley fill or u-
450 PVF; Fig. 4). In the southernmost sector, a fluvial gravel body, $> 3 \text{ m}$ thick, was observed in proximal core
451 14M around 15-18 m depth (Parlagreco et al., 2011 - Fig. 4a). Since this core did not reach the Mutignano Fm
452 substrate, the fluvial gravel body could represent a Holocene fluvial channel deposit of the u-PVF or,
453 alternatively, a buried fluvial terrace generated by repeated fluvial deposition and incision following the MIS
454 5e/MIS 5d transition, as documented for the coeval Biferno “Upper PVF” (Amorosi et al., 2016b). The first
455 interpretation is more likely, because of the presence of overlying “fine-grained sediments rich in wood
456 fragments” (Parlagreco et al., 2011). These latter, in fact, are very similar to the swamp facies identified in
457 core Marconi at the same stratigraphic level (Fig. 4a).

458 The l-PVF, between about 50-38 m depth (Fig. 4a), consists almost entirely of an up to 2 km wide (Fig.
459 4a, b) fluvial gravel deposit, in agreement with classic models (Gibling et al., 2011; Zaitlin et al., 1994). These
460 basal gravels, assigned to the Late Pleistocene on the basis of a radiocarbon date of 11.3 ka cal BP at their top,
461 have maximum thickness of 13 m in the valley depocenter (Figs. 2 and 4a, b). Amalgamation of fluvial bodies
462 decreases upwards, between about 42-33 m depth, with the simultaneous appearance of poorly-drained muds
463 and scattered well-drained and crevasse deposits (Fig. 4a, b).

464 The laterally extensive gravel deposit likely, despite repeated erosional episodes due to fluvial activity
465 within a narrow valley, started to accumulate under lowstand conditions during the LGM (30-19 ka cal BP),
466 when sea-level had dropped down to 120 m (Clark et al., 2009). In the lowermost interval, no preservation of
467 overbank deposits may suggest that fine-grained sediment was completely eroded away by the lateral migration
468 of a (braided?) river system within the narrow LGM valley and transferred to the deep basin. In the uppermost
469 l-PVF (Fig. 4a, b), the occurrence of finer-grained facies and decrease in channel amalgamation are consistent
470 with the gradual evolution of the fluvial system into a meandering alluvial plain during the early deglaciation.
471 Similar changes in fluvial stacking pattern and the decrease in grain size have been linked to the glacial-
472 interglacial transition, which caused significant reduction in stream competence of Holocene river systems
473 compared to their high-energy, LGM counterparts (Amorosi et al., 2017a; Aslan and Autin, 1999; Campo et
474 al., 2016; Kettner and Syvitski, 2008; Macklin et al., 2002; Milli et al., 2016).

475 The u-PVF is about 25 m-thick (38-11 m of reference core depth; Fig. 4a) and mostly composed of non-
476 marine and organic-rich soft deposits (Fig. 4a, b) of Holocene age with Pp values ranging between 0.4-1.8
477 kg/cm². As a whole, the u-PVF records an upward increasing marine influence in its lower interval (11.3-8 ka
478 cal BP), but an opposite trend in the upper part (last 8 ky BP). The early Holocene succession is characterized
479 by the vertical transition from poorly-drained floodplain facies to swamp clays to lagoonal deposits with
480 scattered and narrow (< 100 m wide) distributary-channel sand bodies (Fig. 4a, b). Lagoonal clays identified
481 in the reference core are in lateral transition to coastal sands and swamp deposits in distal and proximal sectors,
482 respectively (Fig. 4b). The vertical facies change from freshwater/swamp to brackish/lagoonal deposits reflects
483 progressive drowning of the valley, between 11.3 and 8 ka cal BP, under conditions of sea-level rise (Lambeck
484 et al., 2011). During this transgressive phase, the Pescara valley drowned, transforming the studied reach into
485 an estuary, as well as already documented for several coastal plains worldwide (Amorosi et al., 2008; Boyd et
486 al., 2006; Dalrymple et al., 1992; Hijma et al., 2009; Hori et al., 2002; Milli et al., 2016, 2013; Ta et al., 2021;
487 Tanabe et al., 2015, 2006; Zaitlin et al., 1994), and in other sectors of the Adriatic basin (Amorosi et al., 2016b;
488 Bruno et al., 2017; De Santis et al., 2020a; Maselli et al., 2014; Ronchi et al., 2021; Rossi et al., 2021). Starting
489 from about 7.8 ka cal BP, lagoonal clays were progressively overlain by swamp facies (Fig. 4a, b). Between
490 7.8 and 7.0 ka cal BP, sea level rose to the elevation of the southern interfluvium (Fig. 4a) and this sector was
491 flooded, causing the progressively widening of paludal areas into the Pescara valley.

492 The uppermost interval (10-0 m depth; Fig. 4a, b) of the Pescara succession is dated to the last 5.2 ky,
493 and reflects transition from lagoonal to poorly-drained depositional environments, up to the modern coastal
494 plain with recent anthropogenic influence (Fig. 4a, b). A sandy fluvial channel-belt, about 500 m-wide (Fig.
495 4a), was identified within this interval. After 5.2 ka cal BP, under nearly stable sea-level conditions (Vacchi et
496 al., 2016), fluvial activity increased (Benito et al., 2015) and the Pescara River likely started to deliver high
497 amounts of sand to the coast, establishing, sustaining and growing a wave-dominated delta with beach ridges
498 developing on either side of the river mouths (Fig. 4b). Subaerially exposed, barrier-beach and deltaic deposits
499 form the uppermost interval (last 3.4 ky; Fig. 4b) of the Pescara coastal plain succession at distal locations of
500 the study area (Urbano et al., 2017). Chronological, sedimentological and paleontological data from Parlagreco
501 et al. (2011) are consistent with this interpretation.

502 The identification of an unconformable relationship between fluvial deposits and subjacent substrate of
503 significantly older age, a methodology generally applied for the identification of ancient PVs (Blum et al.,
504 2013), was also used for the recognition of the late Quaternary Pescara paleovalley fill.

505

506 ***5.2 Sequence stratigraphy***

507 Stratigraphic and chronological data (Figs. 2, 4 and Table 1) allowed to interpret the Late Pleistocene
508 amalgamated fluvial body with a general aggradational stacking pattern as the lowstand systems tract (LST;
509 Fig. 4a, b). The erosional base of the LST gravel body, cutting into considerably (>1 My) older marine substrate
510 corresponds to the classic sequence boundary (SB *sensu* Posamentier et al., 1988; Van Wagoner et al., 1990).
511 At the location of the study area and further down shelf, the SB is genetically linked to the last stage of sea-
512 level fall at the MIS 3-MIS 2 transition (about 30 ka cal BP; Pellegrini et al., 2018, 2017). Between 30-14 ka
513 cal BP, mostly during lowstand conditions, laterally extensive fluvial-channel belts accumulated along the
514 onshore sectors of the Adriatic basin (Amorosi et al., 2016a). The lowstand Pescara River system most likely
515 delivered its fluvial sediments to the MAD basin, about 60 km to the northeast from the modern study area
516 (Fig. 1).

517 Along the southern valley flank, the SB marks the stratigraphic unconformity between the Mutignano
518 Fm and overlying Holocene swamp clays around 12 m depth (core 21; Fig. 4a). In this sector, SB formation
519 could be related to the general phase of fluvial incision caused by the stepwise post-MIS 5e (and pre-MIS 3)
520 sea-level drop. Therefore, from the interfluvial to the depocenter, the SB shows a general diachronous nature
521 (at least post-MIS 5e to MIS 2) that seems to be a characteristic feature of basal valley-fill surfaces, as discussed
522 by Blum et al. (2013). The SB coincides with the paleovalley profile from the main depocenter up to the
523 paleovalley interfluvial (Fig. 4a), where the low-quality data available did not allow the identification of a clear
524 paleosol.

525 The abrupt facies change from the Late Pleistocene l-PVF to the Holocene u-PVF corresponds to the
526 transgressive surface (TS; Fig. 4a, b), which is dated to about 11.3 ka cal BP. The maximum flooding surface
527 (MFS), dated to about 8 ka cal BP (Fig. 4a, b), marks the most landward migration of the barrier-lagoon system,
528 with lagoonal deposits reaching their innermost position about 1.5 km landward of the modern shoreline (Fig.
529 4b). Based on paleontological (micro- and macrofossils) indicators of marine influence in brackish settings,
530 the MFS can be identified quite precisely on the reference core: it corresponds with the deepest-water or higher-
531 salinity facies (i.e., central-lagoon, the sample at 17.6 m depth; Fig. 2), at the turnaround from deepening-
532 upward to shallowing-upward trends (Fig. 4a, b). Hence, the Early Holocene (11.3-8.0 ka cal BP) interval with
533 its characteristic deepening-upward trend, from poorly-drained to “the deepest and highest-salinity” lagoonal
534 facies (Fig. 2), was interpreted as the transgressive systems tract (TST; Fig. 4a, b). On the other hand, the
535 opposite, shallowing-upward trend, from lagoonal to modern coastal plain deposits, shown by the Middle to
536 Late Holocene succession (last 8 ky), allowed its interpretation as the highstand systems tract (HST; Fig. 4a,
537 b). The Middle to Late Holocene succession incidentally corresponds to HST.

538 Unlike the Biferno paleovalley system, located about 80 km south of the study area, where fluvial
539 terraces at various depths were interpreted as the falling stage systems tract (FSST; Amorosi et al., 2016b), no
540 equivalent deposits were identified in the Pescara system. However, the two PVSs share similar characteristics
541 as comparable width (about 2 km) and downstream slope gradient (refer to the Geological Map of Italian Seas
542 at 1:250,000 scale, available at
543 https://www.isprambiente.gov.it/Media/carg/marine/NK_33_5_PESCARA_SOTT/Foglio.html). In the

544 Pescara PVS, gravel bodies that could be interpreted as fluvial terraces have been documented by Desiderio et
545 al. (2007; Fig. 1c) only in the northern sector of the Pescara paleovalley, which was not investigated in this
546 study.

547

548 **6. Millennial-scale architecture and sediment accumulation rates**

549 Seven parasequences (Ps 1-7 in Figs. 4 and 5) were identified and tracked within the whole Holocene
550 succession (TST+HST; Fig. 4a, b). The lowest three parasequences (Ps 1-3; Fig 4a, b) are retrogradationally
551 stacked and form the TST. The uppermost four parasequences (Ps 4-7; Fig. 4a, b), with an aggradational to
552 progradational stacking pattern, make the HST.

553 Parasequence 1 (11.3-9.2 ka cal BP; P1 in Fig. 4), about 12 m thick, is mostly composed of poorly
554 drained floodplain clays. Locally, towards the southern valley flank, scattered well-drained deposits can be
555 found (Fig. 4a). Seawards, poorly drained floodplain sediments are progressively replaced by swamp clays
556 (Fig. 4b). Three minor flooding surfaces were identified at the base of thin swamp intervals within P1 (Fig. 4).
557 The basal flooding surface coincides with the TS (Fig. 4). Mean sediment accumulation rate is 5.7 mm/y (Fig.
558 5).

559 Parasequence 2 (9.2-8.3 ka cal BP; P2 in Fig. 4) is almost completely made up of organic-rich swamp
560 clays, with isolated distributary-channel sand bodies (Fig. 4). No evident downdip facies change can be
561 inferred from the stratigraphic panel of Fig. 4b. P2 has average thickness of 8.5 m (Fig. 4) and exhibits the
562 highest sediment accumulation rate (9.4 mm/y in Fig. 5).

563 Parasequence 3 (8.3-8.0 ka cal BP; P3 in Fig. 4) is characterized by the appearance of lagoonal/outer-
564 estuarine clays in the Pescara valley. Along-dip correlation (Fig. 4b) displays a genetically linked set of
565 freshwater (swamp/inner-estuary), brackish (lagoon/outer-estuary) to nearshore (transgressive barrier?) facies,
566 with an obvious retrogradational trend. P3 shows the minimum thickness (0.75 m) among TST Ps coupled
567 with the lowest accumulation rate (2.5 mm/y; Fig. 5).

568 Parasequence 4 (8.0-7.0 ka cal BP; P4 in Fig. 4) displays a clear shallowing-upward trend (Fig. 4a), with
569 basal (“the deepest”; Fig. 2) lagoonal deposits that are progressively replaced upwards by swamp clays. The

570 internal stacking pattern is generally aggradational (Fig. 4b). The basal flooding surface is the MFS and
571 highlights the transition from retrogradational (TST) to aggradational-to-progradational stacking patterns
572 (HST; Figs. 4b and 5), consistent with the main sequence stratigraphic models described by Catuneanu et al.
573 (2006) and Neal and Abreu (2009). Within P4, a minor flooding surface dated to about 7.8 ka cal BP marks
574 another brackish interval. This deposit is less laterally extensive and includes faunal associations typical of a
575 shallower (inner-lagoon) environment than underlying (outer-estuarine) clays (Fig. 5a, b). P4 is characterized
576 by a mean thickness of about 5.6 m (Fig. 4) and displays a relatively high sediment accumulation rate (5.6
577 mm/y in Fig. 5).

578 Parasequence 5 (7.0-5.2 ka cal BP; P5 in Fig. 4) shows similar facies architecture to P4, with basal
579 lagoonal/outer-estuarine deposits overlain by swamp clays. In contrast, the overall stacking pattern is
580 progradational (Fig. 4b). This parasequence is only 2.4 m-thick (Fig. 4) and marks the lowest sediment
581 accumulation rate of the entire Holocene succession (1.3 mm/y; Fig. 5).

582 Parasequences 6 and 7 (post 5.2 ka cal BP; P6 and P7 in Fig. 4) are the youngest Ps within HST and are
583 characterized by a marked progradational stacking pattern (Fig. 4b). P6 consists entirely of organic-rich swamp
584 clays, whereas P7 includes basal swamp deposits overlain by poorly-drained floodplain and well-drained
585 floodplain facies, in lateral transition to anthropogenic deposits. P7 displays a general increase in the sand/mud
586 ratio, with a fluvial channel-belt sand body (up to 500 m wide) in the central sector of the study area (Fig. 4a)
587 connected with coastal sands basinwards (Fig. 4b). The available data allowed to estimate only a cumulative
588 sediment accumulation rate for P6 and P7, with values of about 1.8 mm/y (Fig. 5).

589 6.1. Sediment accumulation history of the Pescara PVs

590 Similar to what has been documented for the Northern Po-Adriatic sector (Amorosi et al., 2017b),
591 landwards of the shoreline, TST Ps 1-3 generally display the highest accumulation rates (up to 9.4 mm/y; Fig.
592 5), whereas highstand Ps 4-7 are characterized by lower values (down to 1.3 mm/y; Fig. 5). As for their
593 northern equivalent estuarine (TST) deposits, high accumulation rates could reflect generation of
594 accommodation in the Pescara coastal plain due to the eustatic sea-level rise. During the Holocene
595 transgression (11.3-8.0 ka cal BP), for 3.3 ky, the Pescara paleovalley acted as an area of sediment storage.
596 Afterwards, under Late Holocene stable sea-level conditions (HST), sedimentation rates gradually started to

597 decrease, suggesting rapid progradation of coastal systems. During this period, the study area turned into a
598 region of prevailing lateral sediment distribution.

599 On the other hand, the very low sediment accumulation rate of 0.7 mm/y (estimated from the reference
600 core) for the fully-alluvial I-PVF (LST) is not reliable. Accumulation of this unit took place in response to
601 repeated phases of fluvial incision, valley widening, sedimentation and re-incision between 30-11.3 ka cal BP.

602

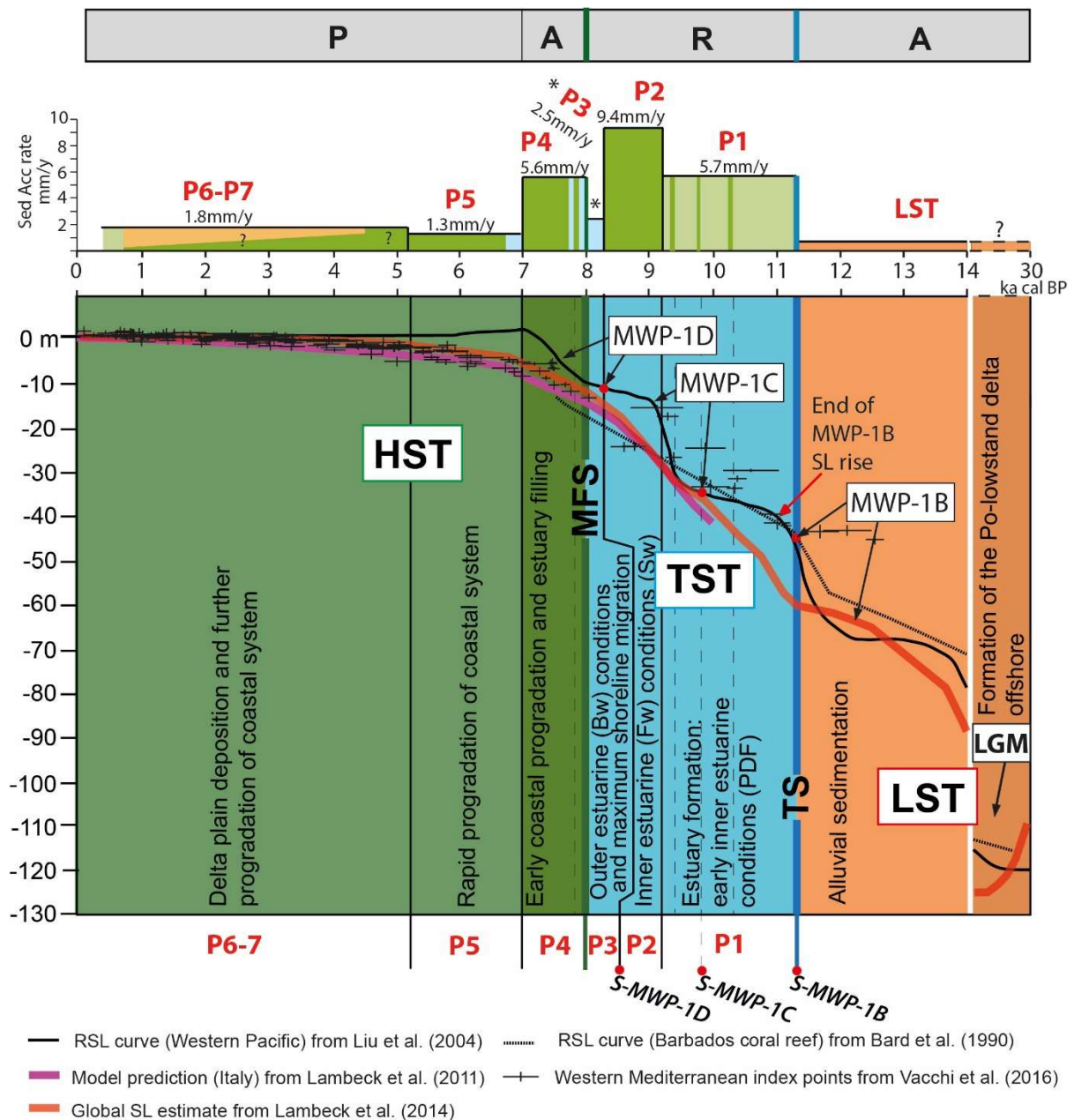
603 **7. Holocene paleoenvironmental evolution and glacio-eustatic control at** 604 **parasequence scale**

605

606 ***7.1 Paleoenvironmental evolution***

607 Comparing the age of retrogradational Ps 1-3 with sea-level curves from the last ca. 11.5 ky (Fig. 5)
608 confirms that the estuary was formed during a phase of eustatic sea-level rise, similar to several coeval estuaries
609 worldwide (Amorosi et al., 2013b; Boyd et al., 2006; Dalrymple et al., 1992; De Santis et al., 2020a; Hijma et
610 al., 2009; Hori et al., 2002; Milli et al., 2016; Ronchi et al., 2021; Ta et al., 2021; Tanabe et al., 2006; Zaitlin
611 et al., 1994). The available data clearly reveal that this phase was punctuated by high-frequency oscillations
612 and short phases of deceleration in relative sea-level rise. Early stages of estuary development (after 11.3 ka
613 cal BP, in proximity of the reference core) were characterized by a general rising of the groundwater table and
614 by the accumulation of poorly-drained floodplain to swamp muds (Fig. 5), with progressively increasing
615 organic matter contents above the TS, as also shown in Figs. 2, 3 and 4. After 9.2 ka cal BP, widespread
616 accumulation of organic-rich facies took place (Fig. 4), and poorly-drained floodplains of P1 were waterlogged
617 due to increasingly higher water table (P2; Fig. 5). Between 9.2 to 8.0 ka BP, the study area was progressively
618 transformed into an estuary characterized in its proximal portion by predominantly freshwater/inner-estuarine
619 conditions (Figs. 4b and 5). Further sea-level rise, between 8.3 and 8.0 ka cal BP, led to the maximum landward
620 migration of a barrier-lagoon systems during deposition of P3 (Fig. 5). This is testified by paleontological data,
621 which show that the “highest-salinity” (brackish) conditions occurred around 8.0 ka cal BP (at the reference
622 core site), and by stratigraphic correlation with coeval coastal sands seawards (core 10, Fig. 4b). At the end of

623 the transgression (onset of P4), with the shoreline in its innermost position, the estuary reached its maximum
624 depth and inland extent (Fig. 4b). Coastal systems then started gradually to prograde basinwards, as suggested
625 by characteristic shallowing-upward cycles of Ps 4-7. During the early aggradational phase recorded by P4,
626 the estuary was progressively filled (Fig. 5). Laterally extensive brackish/outer-estuarine environments
627 developed within the valley, in which sediment was accommodated at relatively high accretion rates (5.6
628 mm/y; Fig. 5), consistent with the aggradational stacking pattern of P4 (Figs. 4a, b and 5). Between 7.0-5.2 ka
629 cal BP (P5), brackish environments were replaced by freshwater conditions in inland sectors of the study area
630 (Figs. 4 and 5). At that time, as suggested by markedly lower sedimentation rates (1.3 mm/y in the reference
631 core; Fig. 5), by the reduced parasequence thickness (Fig. 4a) and by the clear progradational stacking pattern
632 of P5 (Figs. 4b and 5), progradation of the coastal system quickened. In the last 5.2 ky (Ps 6-7), the study area
633 experienced delta plain aggradation and further progradation of the coastal system (Fig. 5). Additional
634 stratigraphic and chronological data from the relatively distal core 14M (Parlagreco et al., 2011; Fig. 1 for
635 location) confirm that fluvio-deltaic sands accumulated during the last 4 ky as a result of the interaction
636 between fluvial (Pescara River) and marine processes. The northeastern sector of the study area was probably
637 characterized by a fluvio-deltaic system frequently exposed to high-energy coastal dynamics. Interestingly,
638 based on the ages of the P6 basal flooding surface (about 5.2 ka cal BP) and of the MFS offshore (“a regional
639 downlap surface” marking the base of the HST prograding wedge and dated $6,160 \pm 60$ cal ky BP; Asioli et al.,
640 1996; Trincardi et al., 1996), P6 and P7 are supposed to be coeval of the HST prograding wedge documented
641 offshore the Apennine coast (Cattaneo et al., 2003).



642

643

644

645

646

647

648

649

650

Fig. 5 – Comparison between millennial-to submillennial-scale sediment accumulation rates (Sed Acc rate) with indication of prevailing facies association (refer to Fig. 4 for legend), LGM to post-glacial sea-level curves from the Western Pacific (Liu et al., 2004), the Atlantic (Bard et al., 1990), the Mediterranean area (Lambeck et al., 2011) and the global one (Lambeck et al., 2014). Timing of parasequences (in red) evolution within the Pescara paleovalley system. Relative sea-level (RSL) index points from tectonically stable areas of the western Mediterranean are from Vacchi et al. (2016). LST: lowstand systems tract; TST: transgressive systems tract; HST: highstand systems tract; TS: Transgressive surface; MFS: Maximum flooding surface; LGM: Last Glacial Maximum; MWP: Melt water Pulse; S-MWP: Melt water pulse surface; A: aggradational

651 *stacking pattern; R: retrogradational stacking pattern; P: progradational stacking pattern; Bw: brackish*
652 *water; Fw: freshwater; SL: sea-level. Modified after Amorosi et al. (2017b).*

653

654 ***7.2 Influence of post-Younger Dryas episodes of glacio-eustatic sea-level rise***

655 ***7.2.1. Melt Water Pulse 1B***

656 Early Holocene poorly-drained conditions (P1) have also been documented for coeval (post-12 ka cal
657 BP) successions within the Adriatic basin as the Biferno PVF (Amorosi et al., 2016b) and the Emilia-Romagna
658 coastal sector (P1 of Amorosi et al., 2017b). Comparable and coeval transitional deposits between alluvial and
659 fully-estuarine have also been recognized outside the Adriatic domain, beneath the Tyrrhenian coastal plains
660 (Amorosi et al., 2008; Milli et al., 2016) but also worldwide from Northern Europe to the Asian coasts (Hijma
661 et al., 2009; Tanabe et al., 2015; Hori et al., 2002). The basal surface of P1 is the TS: this surface, dated to
662 about 11.3 ka cal BP, clearly marks the end of a remarkable phase of fluvial activity, as suggested by the
663 upward change in fluvial stacking pattern atop LST deposits (Fig. 4), also illustrated by Campo et al. (2017)
664 from the Po coastal succession. Chronological and stratigraphic data make the TS correlative offshore with the
665 Melt Water Pulse (MWP) 1B (Fairbanks, 1989; Liu et al., 2004) surface (Zecchin et al., 2015; their Fig. 8).
666 This latter, in turn, coincides with the “S2 surface” of Maselli et al. (2011) that separates middle from upper-
667 TST units and that marks the end of a short-lived episode of subaqueous progradation assigned to the Younger
668 Dryas reversal (i.e., 12.9-11.6 ka cal BP; Cheng et al., 2020). The P1 flooding event, thus, could have been
669 triggered by the post-Younger Dryas sea-level rise linked to the MWP-1B dated to about 11.6-11.3 ka cal BP
670 (Fairbanks, 1989; Fig. 5). MWP-1B is not well documented as MWP-1A, and defined as elusive in far-field
671 sea-level records (Lambeck et al., 2014; Harrison et al., 2019; Tian et al., 2020). Abrupt change in fluvial
672 stacking pattern and rapid establishment of inner-estuarine conditions documented for the Pescara coastal
673 plain, along with data presented by Amorosi et al. (2017b) for the northern sector, strongly support evidences
674 of the MWP-1B effects in the Mediterranean Sea. An estimated sea-level about 50 m below the present, around
675 11.3 ka cal BP (Lambeck et al., 2014, their Fig. 4), is only seemingly inconsistent contrast with the TS elevation
676 (between 43-33 m bsl, Fig. 4b), for the following reasons: (i) possible unreliability of the sea-level curve
677 (Lambeck et al., 2014) that does not take into account data from the Mediterranean Sea (their Fig. 1); (ii) the

inland position of the study area (Fig. 1); (iii) the steepness of the Central Adriatic shelf (0.2° ; Maselli et al., 2011). As for this latter aspect, the TS shows a remarkable change in elevation (10 m in less than 2 km; see Fig. 4b). As regard the position of the study area with respect to the coastline at about 11.3 ka cal BP, this is supported by the non-marine facies associations of P1 (poorly drained floodplain and swamp). Within P1, a minor flooding dated to 10.3 ka cal BP is coeval with a barrier lagoon system identified in the northern Adriatic shelf by Storms et al. (2008) which was not correlated to the MWP-1B. On the contrary, MWP-1B sea-level rise effects have been documented in the Southern Adriatic, Manfredonia Gulf, by De Santis et al. (2020b). Here, MWP-1B has been thought to have caused the drowning and overstepping of previous coastal systems and the formation of a wave ravinement surface.

7.2.2. *Melt Water Pulse 1C*

Correlation of the overall stratigraphy with the sea-level curves (Fig. 5) documents the possible link between the minor flooding surface dated to about 9.8 ka cal BP and the beginning of MWP-1C, whereas the 9.4 cal ky BP flooding is simultaneous to the coeval glacio-eustatic event. Following Zecchin et al. (2015), the 9.8 ky BP flooding has been labelled as the MWP-1C surface (S-MWP1C of Fig. 5). Major effects of the post-MWP-1C sea-level rise are distinctly recorded by P2, which shows the most widespread landward incursion of inner-estuarine environments in the study area. Comparable remarkable effects of the post-MWP 1C sea-level rise are well documented in the Northern Adriatic sector. In the Po coastal Plain, Amorosi et al. (2017b) and Bruno et al. (2017) showed the widespread landward incursion of inner-estuarine environments. The age of their P2 is almost identical (9.2-7.7 ka cal BP) to the age of the Pescara parasequence P2 (9.2-8.3 ka cal BP; Fig. 5). Similarly, in the Tagliamento River Plain, Ronchi et al. (2021) dated to about the same age interval (9.4 to 8.4 ky BP) equivalent organic-rich deposits termed as “basal-peat”. To the south, the Biferno VF (Amorosi et al., 2016b), between 18 and 11 m depth, is also characterized by a coeval and predominantly swampy interval. As for the Pescara P2, the top of this interval is dated to about 8.3 ka cal BP ($8,264 \pm 65$ ka cal BP; their Fig. 5). Even more interesting, is the chronological equivalence with the “Eu-transgressive unit” of the Manfredonia Gulf, dated to 9.2-8.3 ka cal BP (De Santis et al., 2020a). Similar successions have been documented for the Tyrrhenian coast (Amorosi et al., 2013a), and worldwide in the Rhine Delta (Amorosi et al., 2013b), in the Song Hong River (Hori et al., 2004) and the Pearl River (Zong et al., 2009). As different

sectors of the Adriatic Sea and coastal plain successions around the world recorded concomitant deposition of similar organic-rich facies associations, it seems that post MWP-1C sea-level rise played a key role as eustatic factor not only at the basin-scale (Adriatic) but also globally.

7.2.3. *Melt Water Pulse 1D*

The transition to P3 marks the establishment of brackish environments in the study area. The basal P3 flooding was identified as the MWP-1D surface (MWP1D-S of Fig. 5), because it post-dates an 8.3 ka cal BP swamp deposit (Fig. 4). The Biferno and the Po coastal Plain successions present similar ages (about 8.3 ka cal BP) for the transition from swamp (inner-estuarine) strata to overlying brackish (outer-estuarine) deposits, dated to 8.0-7.7 ka cal BP respectively (Amorosi et al., 2017b, 2016b). Most likely MWP-1D produced the maximum landward migration of the barrier-lagoon systems, around 8.0-7.7 ka cal BP, as recorded for the study area (Figs. 4 and 5), for different sectors of the Adriatic (Amorosi et al., 2017b, 2016b; Ronchi et al., 2021) and beyond (Amorosi et al., 2013a, b). The age of the MFS is consistent with the 8.0-7.0 ka cal BP age documented for the same surface in several coastal successions (Amorosi et al., 2008; Breda et al., 2016; Hori et al., 2004; Milli et al., 2013; Tanabe, 2020; Tanabe et al., 2022, 2015). In particular, it matches the age of the MFS in the Biferno PVs (Amorosi et al., 2016b) and in the northern Adriatic sector (Amorosi et al., 2017b). A possible alternative position for the MFS is within P4 (i.e., intra parasequence) atop lagoonal deposits dated to 7.8 ka cal BP (Figs. 4 and 5). An age of about 7.7 ka cal BP fits the MFS age reported from different coastal successions mentioned above, especially the MFS documented from Amorosi et al. (2017b). As reported by Tanabe (2020), analogous sea-level rise events have been inferred for MWP-1D between 7.8 and 6.8 ka cal BP for different locations worldwide (Blanchon et al., 2002; Bird et al., 2007; Song et al., 2018; Yu et al., 2007). Comparison of sea-level curve from Lambeck et al. (2011) and index points from Vacchi et al. (2016; Fig. 5) shows that in the Mediterranean Sea, the maximum sea-level jump linked to the MWP-1D ended about 7.5 ka cal BP (Fig. 5). The effects of the flooding driven by MWP-1D are not recorded after 7.0 ka cal BP, when sea-level stabilized (Fig. 5). According to our reconstruction, the 7.0 ka cal BP flooding and its correlative lagoonal deposits likely represent the very “last ditch effort” of MWP-1D in this sector of the Adriatic before coastal system progradation took place.

731 The Pescara Holocene succession (TST+HST) has many similarities in terms of facies architecture with
732 coeval successions along the Adriatic basin and worldwide (Amorosi et al., 2017b; Milli et al., 2016; Ruberti
733 et al., 2018; Hijma et al., 2009; Tanabe et al., 2006; Hori et al., 2002; Blum et al., 1995; Blum and Aslan, 2006;
734 Blum and Price, 1998; Payenberg et al., 2006; Rittenour et al., 2007; Thomas and Anderson, 1994; Ronchi et
735 al., 2021; Jessen et al., 2008; Shaver and Pusc, 1992; Seifert et al., 2008; Hickin and Best, 2013; Barnes et al.,
736 2021; Goetz et al., 2021; Ta et al., 2021), confirming the basin-scale importance of the eustatic component as
737 the major controlling factor during Termination 1 (Denton et al., 2010).

738 As a whole, this investigation has documented a clear influence of the stepwise sea-level jumps caused
739 by the MWPs 1B, 1C, and 1D on the stratigraphic architecture of the Pescara paleovalley fill. These events are
740 still considered as local phenomena by some authors (see Tanabe, 2020), because their effects were not
741 identified globally and there is not yet full consensus on their timing and magnitude. However, as also reported
742 in this study, many works documented that eustatic rise episode was not smooth and gradual, but punctuated.
743 Compared to MWPs 1A and 1B (Bard et al., 2010; Abdul et al., 2016; Tian et al., 2020), MWPs 1C and 1D
744 are thought to have been less marked (Zecchin et al., 2015) and poorly documented, especially in the
745 Mediterranean area, as previously documented by Amorosi et al (2017b) for the Northern Adriatic. Hence, this
746 study provides data for future refinements of the post-LGM sea-level curve for this Mediterranean sector.

747

748 **8. Conclusions**

749 A buried paleovalley system (PVS), about 50 m deep and up to 2 km wide, was recognized beneath the
750 Pescara coastal plain through stratigraphic correlation based on sedimentological, paleontological (meiofauna
751 and mollusks), chronological and geotechnical (pocket penetrometer measurements) data. Detailed facies
752 analysis was carried out on a 52 m-long core specifically recovered in the valley depocenter.

753 Two NE-SE and SW-NE oriented stratigraphic panels provided the 3D-facies architecture of the Late
754 Pleistocene-Holocene paleovalley fill (PVF), and allowed the reconstruction of the paleovalley profile, incised
755 into Calabrian age marine deposits. The general facies architecture and fluvial stacking patterns resemble the
756 stratigraphic organization of several ancient and Quaternary paleovalley systems worldwide, with the lower

757 paleovalley fill (l-PVF), composed of up to 13-m-thick, amalgamated fluvial gravel bodies of Late Pleistocene
758 age (30-pre-11.3 ka cal BP), interpreted as the lowstand systems tract (LST), because of its overall
759 aggradational stacking.

760 The mud-dominated, Holocene upper paleovalley fill (u-PVF) with isolated sand bodies is about 25 m-
761 thick and consists mostly of non-marine, organic-rich deposits with low pocket penetrometer values (0.4-1.8
762 g/cm²). The vertical transition from poorly-drained floodplain facies to swamp clays to lagoonal deposits
763 reflects progressive drowning of the valley and formation of an estuary, as a result of the Holocene
764 transgression. During the last 8.0 ky, the estuary was progressively filled up to the establishment of the modern
765 wave-dominated delta plain environment.

766 The abrupt facies change from the Late Pleistocene l-PVF to the Holocene u-PVF corresponds to the
767 transgressive surface (TS), dated to about 11.3 ka cal BP. The early Holocene (11.3-8.0 ka cal BP) interval
768 with a deepening-upward trend represents the transgressive systems tract (TST). The maximum flooding
769 surface (MFS), dated to about 8.0 ka cal BP was tracked at the turnaround from deepening-upward to
770 shallowing-upward trend and marks the maximum landward migration of barrier-lagoon systems, with outer-
771 estuarine deposits reaching their innermost position up to 1.5 km landward of the modern shoreline. The last
772 8.0 ky succession, with a characteristic shallowing-upward trend from estuarine to modern delta plain deposits,
773 is interpreted as the highstand systems tract (HST). The age of the MFS is consistent with the 8.0-7.0 ka cal
774 BP age documented for the same surface in several coastal successions worldwide.

775 Seven parasequences (Ps 1-7) were identified and tracked within the Holocene interval (TST+HST).
776 The lower three (Ps 1-3) are retrogradationally stacked and form the TST, whereas the uppermost four (Ps 4-
777 7) with peculiar aggradational to progradational stacking pattern make the HST. Based upon paleontological
778 data and consistent with the stacking pattern of parasequences (etrogradational-aggradational to
779 progradational), the MFS is places between 8.0 ka cal and 7.7 ka cal BP. However, its positioning can be
780 debated and, an alternative position beyond parasequences and flooding boundaries could be within P4, at the
781 transition from lagoonal and swamp deposits, dated to about 7.7 ka cal BP.

782 Transgressive Ps 1-3 record the overall drowning of the valley and the onset of estuarine conditions.
783 Due to the general sea-level rise, progressively deeper conditions, from inner- (Ps 1-2) to outer-estuarine (P3),

were established in the study area. Between 8.0-7.0 ka cal BP sea-level stabilized and once the estuary was filled with freshwater organic-rich deposits (aggradational P4), coastal progradation definitively started (P5). In the last 5.2 ka cal BP (Ps 6-7) further coastal progradation took place. Coastal plain facies accumulated landward, whereas a wave-dominated fluvio-deltaic system developed at distal locations.

In general, TST parasequences display higher accumulation rates (up to 9.4 mm/y) than HST ones. These latter are characterized by a mean value of about 2.9 mm/y. High-sediment accumulation rates may reflect generation of accommodation caused by the rapid eustatic sea-level rise. On the other hand, under highstand conditions, sedimentation rates progressively decreased suggesting rapid progradation of the coastal system basinwards.

The Pescara PVS is the first example of late Quaternary PVs identified in front of the Mid-Adriatic Depression (MAD) basin, and represents the essential “onshore component” of the Adriatic system in a source-to-sink (S2S) perspective. The paleovalley, from a region of sediment storage during the transgression (11.3-8.0 ka cal BP) turned into a sector of prevailing lateral sediment distribution under highstand conditions (last 8.0 ky).

A first correlation with offshore data and comparison with coeval successions along the Adriatic basin (and worldwide) show many similarities in terms of facies/stratigraphic architecture and confirm the key role of eustatic sea-level rise as the major controlling factor during the post-LGM transgression, providing new evidence for Melt Water Pulses (MWP) 1B, 1C and 1D. The eustatic rise linked to MWP-1B reasonably triggered the P1 flooding event and the first establishment of inner-estuarine conditions tens of kilometers landwards of the coastline.

The Pescara valley fill also records the influence of minor and still poorly documented around the world MWP 1C and 1D. Whilst the minor 9.8 ka cal BP flooding surface was linked to the beginning of MWP-1C, major effects of the post-MWP-1C sea-level rise in the study area are clearly recorded by P2. Similar to what was documented for several coeval successions of the Adriatic, P2 is characterized by the most widespread landward incursion of inner-estuarine deposits in the study area. The onset of MWP-1D is marked by the basal P3 flooding that highlights the onset of the very last backstepping episode of a barrier-lagoon system in this Central Adriatic sector, consistent with data from Amorosi et al. (2017b) for the Northern Adriatic. Hence,

811 MWP-1D can be considered as the most important trigger for the maximum landward migration of the
812 shoreline at the basin-scale.

813

814 **Authors contribution**

815 Bruno Campo: conceptualization, methodology, formal analysis, investigation, data curation, writing -
816 original draft, visualization, project administration. Barbieri Giulia: formal analysis, investigation. Di Martino
817 Andrea: investigation. Hong Wan: formal analysis. Scarponi Daniele: formal analysis, writing review &
818 editing. Vaiani Stefano Claudio: formal analysis, writing review & editing. Amorosi Alessandro: supervision,
819 writing review & editing, project administration, funding acquisition.

820

821 **Acknowledgements**

822 This work was supported by the Italian Ministry of University and Research under the PRIN 2017
823 program, project number 2017ASZAKJ “*The Po-Adriatic Source-to-Sink system (PASS): from modern*
824 *sedimentary processes to millennial-scale stratigraphic architecture*”, grant to Prof. Alessandro Amorosi. We
825 are grateful to the two anonymous reviewers for their very useful and constructive comments.

826

827 **References**

828

829 Abdul, N.A., Mortlock, R.A., Wright, J.D., Fairbanks, R.G., 2016. Younger Dryas sea level and meltwater
830 pulse 1B recorded in Barbados reef crest coral *Acropora palmata*. *Paleoceanography* 31, 330–344.

831 Aguzzi, M., Amorosi, A., Colalongo, M.L., Lucchi, M.R., Rossi, V., Sarti, G., Vaiani, S.C., 2007. Late
832 Quaternary climatic evolution of the Arno coastal plain (Western Tuscany, Italy) from subsurface
833 data. *Sediment. Geol.* 202, 211–229. <https://doi.org/10.1016/j.sedgeo.2007.03.004>

834 Allen, G.P., Posamentier, H.W., 1993. Sequence stratigraphy and facies model of an incised valley fill: the

835 Gironde Estuary, France. *J. Sediment. Petrol.* 63, 378–391.

836 Amorosi, A., Bracone, V., Campo, B., D’Amico, C., Rossi, V., Roszkopf, C.M., 2016b. A late Quaternary
837 multiple paleovalley system from the Adriatic coastal plain (Biferno River, Southern Italy).
838 *Geomorphology* 254, 146–159. <https://doi.org/10.1016/j.geomorph.2015.11.023>

839 Amorosi, A., Rossi, V., Sarti, G. and Mattei, R., 2013a. Coalescent valley fills from the late Quaternary
840 record of Tuscany (Italy). *Quaternary International*, 288, pp.129-138.

841 Amorosi, A., Rossi, V. and Vella, C., 2013b. Stepwise post-glacial transgression in the Rhône Delta area
842 as revealed by high-resolution core data. *Palaeogeography, Palaeoclimatology, Palaeoecology*,
843 374, pp.314-326.

844 Amorosi, A., Maselli, V., Trincardi, F., 2016a. Onshore to offshore anatomy of a late Quaternary source-
845 to-sink system (Po Plain-Adriatic Sea, Italy). *Earth-Science Rev.* 153, 212–237.
846 <https://doi.org/10.1016/j.earscirev.2015.10.010>

847 Amorosi, A., Bruno, L., Cacciari, M., Campo, B., Rossi, V., 2021. Tracing marine flooding surface
848 equivalents across freshwater peats and other wetland deposits by integrated sedimentological and
849 pollen data. *Int. J. Coal Geol.* 246, 103830. <https://doi.org/10.1016/j.coal.2021.103830>

850 Amorosi, A., Bruno, L., Campo, B., Morelli, A., Rossi, V., Scarponi, D., Hong, W., Bohacs, K.M. and
851 Drexler, T.M., 2017b. Global sea-level control on local parasequence architecture from the
852 Holocene record of the Po Plain, Italy. *Mar. Pet. Geol.* 87, 99-111.

853 Amorosi, A., Bruno, L., Cleveland, D.M., Morelli, A., Hong, W., 2017a. Paleosols and associated channel-
854 belt sand bodies from a continuously subsiding late quaternary system (Po basin, Italy): New
855 insights into continental sequence stratigraphy. *Bull. Geol. Soc. Am.* 129, 449–463.
856 <https://doi.org/10.1130/B31575.1>

857 Amorosi, A., Bruno, L., Campo, B., Morelli, A., 2015. The value of pocket penetration tests for the high-
858 resolution palaeosol stratigraphy of late Quaternary deposits. *Geol. J.* 50, 670–682.

859 Amorosi, A., Pacifico, A., Rossi, V., Ruberti, D., 2012. Late Quaternary incision and deposition in an active

860 volcanic setting: The Volturno valley fill, southern Italy. *Sediment. Geol.* 282, 307–320.
861 <https://doi.org/10.1016/j.sedgeo.2012.10.003>

862 Amorosi, A., Ricci Lucchi, M., Rossi, V., Sarti, G., 2009. Climate change signature of small-scale
863 parasequences from Lateglacial-Holocene transgressive deposits of the Arno valley fill.
864 *Palaeogeogr. Palaeoclimatol. Palaeoecol.* 273, 142–152.
865 <https://doi.org/10.1016/j.palaeo.2008.12.010>

866 Amorosi, A., Rossi, V., Sarti, G., Mattei, R., 2013a. Coalescent valley fills from the late Quaternary record
867 of Tuscany (Italy). *Quat. Int.* 288, 129–138. <https://doi.org/10.1016/j.quaint.2011.10.015>

868 Amorosi, A., Rossi, V., Vella, C., 2013b. Stepwise post-glacial transgression in the Rhône Delta area as
869 revealed by high-resolution core data. *Palaeogeogr. Palaeoclimatol. Palaeoecol.* 374, 314–326.

870 Amorosi, A., Rossi, V., Scarponi, D., Vaiani, S.C., Ghosh, A., 2014. Biosedimentary record of postglacial
871 coastal dynamics: High-resolution sequence stratigraphy from the northern Tuscan coast (Italy).
872 *Boreas* 43, 939–954. <https://doi.org/10.1111/bor.12077>

873 Amorosi, A., Sarti, G., Rossi, V., Fontana, V., 2008. Anatomy and sequence stratigraphy of the late
874 Quaternary Arno valley fill (Tuscany, Italy). *GeoActa* 117–128.

875 Antonioli, F., Ferranti, L., Fontana, A., Amorosi, A., Bondesan, A., Braitenberg, C., Dutton, A., 2009.
876 Holocene relative sea-level changes and vertical movements along the Italian and Istrian coastlines.
877 *Quat. Int.* 206, 102–133. <https://doi.org/10.1016/j.quaint.2008.11.008>

878 Ascione, A., Cinque, A., Miccadei, E., Villani, F., Berti, C., 2008. The Plio-Quaternary uplift of the
879 Apennine chain: new data from the analysis of topography and river valleys in Central Italy.
880 *Geomorphology* 102, 105–118. <https://doi.org/10.1016/j.geomorph.2007.07.022>

881 Asioli, A., 1996. High resolution foraminifera biostratigraphy in the Central Adriatic basin during the last
882 deglaciation: a contribution to the PALICLAS Project. *Memorie-Istituto Ital. di Idrobiol.* 55, 197–
883 218.

- Aslan, A., Autin, W.J., 1999. Evolution of the Holocene Mississippi River floodplain, Ferriday, Louisiana: insights on the origin of fine-grained floodplains. *J. Sediment. Res.* 69, 800-815.
- Aslan, A., Blum, M.D., 1999. Contrasting styles of Holocene avulsion, Texas Gulf Coastal Plain, in: Smith, N.D., Rogers, J.J. (Eds.), *Fluvial Sedimentology VI. IAS Special Publication*, 28, pp. 193-209.
- Athersuch, J., Horne, D.J., Whittaker, J.E., 1989. Marine and brackish water ostracods (superfamilies Cypridacea and Cytheracea): keys and notes for the identification of the species. Brill Archive, Leiden.
- Azzarone, M., Pellegrini, C., Barbieri, G., Rossi, V., Gamberi, F., Trincardi, F., Scarponi, D., 2020. Linking benthic fauna and seismic facies to improve stratigraphic reconstructions: The case of the mid-adriatic deep since the late glacial period (central adriatic sea). *Boll. della Soc. Paleontol. Ital.* 59, 9–23. <https://doi.org/10.4435/BSPI.2020.03>
- Barbieri, G., Rossi, V., Vaiani, S.C., Dasgupta, U., Amorosi, A., 2021. Quantitative paleoecology in shallow-marine settings: The value of ostracods and foraminifers from the Holocene North Adriatic record. *Palaeogeogr. Palaeoclimatol. Palaeoecol.* 572, 110408. <https://doi.org/10.1016/j.palaeo.2021.110408>
- Barbieri, G., Vaiani, S.C., 2018. Benthic foraminifera or Ostracoda? Comparing the accuracy of palaeoenvironmental indicators from a Pleistocene lagoon of the Romagna coastal plain (Italy). *J. Micropalaeontology* 37, 203–230. <https://doi.org/10.5194/jm-37-203-2018>
- Bard, E., Hamelin, B., Delanghe-Sabatier, D., 2010. Deglacial meltwater pulse 1B and Younger Dryas sea levels revisited with boreholes at Tahiti. *Science* (80-.). 327, 1235–1237.
- Bard, E., Hamelin, B., Fairbanks, R.G., 1990. U-Th ages obtained by mass spectrometry in corals from Barbados: sea level during the past 130,000 years. *Nature* 346, 456–458.
- Barnes, H., Hinojosa, J.R., Spinelli, G.A., Mozley, P.S., Koning, D., Sproule, T.G., Wilson, J.L., 2021. Detecting fault zone characteristics and paleovalley incision using electrical resistivity: Loma Blanca Fault, New Mexico. *Geophysics* 86, B209–B221.

- Bellotti, P., Caputo, C., Davoli, L., Evangelista, S., Garzanti, E., Pugliese, F., Valeri, P., 2004. Morpho-sedimentary characteristics and Holocene evolution of the emergent part of the Ombrone River delta (southern Tuscany). *Geomorphology* 61, 71–90. <https://doi.org/10.1016/j.geomorph.2003.11.007>
- Benito, G., Macklin, M.G., Panin, A., Rossato, S., Fontana, A., Jones, A.F., Machado, M.J., Matlakhova, E., Mozzi, P., Zielhofer, C., 2015. Recurring flood distribution patterns related to short-term Holocene climatic variability. *Sci. Rep.* 5, 1–8. <https://doi.org/10.1038/srep16398>
- Bhattacharya, J.P., 2006. Deltas, in: Posamentier, H.W., Walker, R.G. (Eds.), *Facies Models Revisited*. SEPM Society for Sedimentary Geology, pp. 237–292. <https://doi.org/10.2110/pec.06.84.0237>
- Bhattacharya, J.P., Copeland, P., Lawton, T.F., Holbrook, J., 2016. Estimation of source area, river paleo-discharge, paleoslope, and sediment budgets of linked deep-time depositional systems and implications for hydrocarbon potential. *Earth-Science Rev.* 153, 77–110.
- Bigi, S., Cantalamessa, G., Centamore, E., Didaskalu, P., Dramis, F., Farabollini, P., Gentili, B., Invernizzi, C., Micarelli, A., Nisio, S., Pambianchi, G., Potetti, M., 1995. La fascia periadriatica marchigiano-abruzzese dal Pliocene medio ai tempi attuali: evoluzione tettonico-sedimentaria e geomorfologica. *Studi Geologici Camerti Special volume*, 37–49.
- Bird, M.I., Fifield, L.K., Teh, T.S., Chang, C.H., Shirlaw, N., Lambeck, K., 2007. An inflection in the rate of early mid-Holocene eustatic sea-level rise: A new sea-level curve from Singapore. *Estuar. Coast. Shelf Sci.* 71, 523–536.
- Bishop, D., 2010. New approaches to understanding the structure and geotechnical characteristics of estuarine sediments. *Aust. Geomech.* 45, 111.
- Blanchon, P., Jones, B., Ford, D.C., 2002. Discovery of a submerged relic reef and shoreline off Grand Cayman: further support for an early Holocene jump in sea level. *Sediment. Geol.* 147, 253–270.

- Blockley, S.P.E., Lowe, J.J., Walker, M.J.C., Asioli, A., Trincardi, F., Coope, G.R., Donahue, R.E., 2004. Bayesian analysis of radiocarbon chronologies: examples from the European Late-glacial. *J. Quat. Sci.* 19, 159–175.
- Blum, M.D., Aslan, A., 2006. Signatures of climate vs. sea-level change within incised valley-fill successions: Quaternary examples from the Texas GULF Coast. *Sediment. Geol.* 190, 177–211. <https://doi.org/10.1016/j.sedgeo.2006.05.024>
- Blum, M.D., Martin, J., Milliken, K., Garvin, M., 2013. Paleovalley systems: Insights from Quaternary analogs and experiments. *Earth-Science Rev.* 116, 128–169. <https://doi.org/10.1016/j.earscirev.2012.09.003>
- Blum, M.D., Morton, R.A., Durbin, J.M., 1995. Deweyville” terraces and deposits of the Texas Gulf coastal plain. *Gulf Coast Assoc. Geol. Soc. Trans.* 45, 53–60.
- Blum, M.D., Price, D.M., 1998. Quaternary alluvial plain construction in response to glacio-eustatic and climatic controls, Texas Gulf coastal plain, in: Shanley, K.W., McCabe, P.J. (Eds.), *Relative Role of Eustasy, Climate and Tectonism in Continental Rocks*. SEPM Special Publication, 59, pp. 31–48.
- Blum, M.D., Törnqvist, T.E., 2000. Fluvial responses to climate and sea-level change: A review and look forward. *Sedimentology* 47, 2–48. <https://doi.org/10.1046/j.1365-3091.2000.00008.x>
- Blum, M.D., Womack, J.H., 2009. Climate change, sea-level change, and fluvial sediment supply to deepwater systems, in: Kneller, B., Martinsen, O.J., McCaffrey, B. (Eds.), *External Controls on Deep Water Depositional Systems: Climate, Sea-Level, and Sediment Flux*. SEPM Special Publication, 92, pp. 15-39.
- Boyd, R., Dalrymple, R.W., Zaitlin, B.A., 2006. Estuarine and incised-valley facies models, in: Posamentier, H.W., Walker, R.G. (Eds.), *Facies Models Revisited*. SEPM Special Publication 84, pp. 171-235.
- Boyd, R., Suter, J., Penland, S., 1989. Relation of sequence stratigraphy to modern sedimentary

- environments. *Geology* 17, 926–929. [https://doi.org/10.1130/0091-7613\(1989\)017<0926:ROSSTM>2.3.CO;2](https://doi.org/10.1130/0091-7613(1989)017<0926:ROSSTM>2.3.CO;2)
- Bracone, V., Amorosi, A., Auceili, P.P.C, Ciampo, G., Di Donato, V., Roskopf, C., 2012b. Palaeoenvironmental evolution of the Plio-Pleistocene Molise Periadriatic Basin (Southern Apennines, Italy): Insight from Montesecco Clays. *Ital. J. Geosci.* 131, 272–275. <https://doi.org/10.3301/IJG.2012.20>
- Bracone, V., Amorosi, A., Auceili, P.P.C., Roskopf, C.M., Scarciglia, F., Di Donato, V., Esposito, P., 2012a. The Pleistocene tectono-sedimentary evolution of the Apenninic foreland basin between Trigno and Fortore rivers (Southern Italy) through a sequence-stratigraphic perspective. *Basin Res.* 24, 213–233. <https://doi.org/10.1111/j.1365-2117.2011.00523.x>
- Breda, A., Amorosi, A., Rossi, V., Fusco, F., 2016. Late-glacial to holocene depositional architecture of the ombrone palaeovalley system (Southern Tuscany, Italy): Sealevel, climate and local control in valley-fill variability. *Sedimentology* 63, 1124–1148. <https://doi.org/10.1111/sed.12253>
- Bridge, J.S., 2006. Fluvial facies models: recent developments, in: Posamentier, H., Walker, R.G. (Eds.), *Facies Models Revisited*. SEPM Special Publication 84, pp. 85–170.
- Bruno, L., Bohacs, K.M., Campo, B., Drexler, T.M., Rossi, V., Sammartino, I., Scarponi, D., Hong, W., Amorosi, A., 2017. Early Holocene transgressive palaeogeography in the Po coastal plain (northern Italy). *Sedimentology* 64, 1792–1816. <https://doi.org/10.1111/sed.12374>
- Bruno, L., Campo, B., Di Martino, A., Hong, W., Amorosi, A., 2019. Peat layer accumulation and post-burial deformation during the mid-late Holocene in the Po coastal plain (Northern Italy). *Basin Res.* 31, 621–639. <https://doi.org/10.1111/bre.12339>
- Buck, C.E., Higham, T.F.G., Lowe, D.J., 2003. Bayesian tools for tephrochronology. *The Holocene* 13, 639–647.
- Buck, C.E., Kenworthy, J.B., Litton, C.D., Smith, A.F.M., 1991. Combining archaeological and radiocarbon information: a Bayesian approach to calibration. *Antiquity* 65, 808–821.

982 Buck, C.E., Litton, C.D., Smith, A.F.M., 1992. Calibration of radiocarbon results pertaining to related
 983 archaeological events. *J. Archaeol. Sci.* 19, 497–512.

984 Busschers, F.S., Kasse, C., van Balen, R.T., Vandenberghe, J., Cohen, K.M., Weerts, H.J.T., Wallinga, J.,
 985 Johns, C., Cleveringa, P., Bunnik, F.P.M., 2007. Late Pleistocene evolution of the Rhine-Meuse
 986 system in the southern North Sea basin: imprints of climate change, sea-level oscillation and glacio-
 987 isostasy. *Quat. Sci. Rev.* 26, 3216–3248. <https://doi.org/10.1016/j.quascirev.2007.07.013>

988 Busschers, F.S., Weerts, H.J.T., Wallinga, J., Cleveringa, P., Kasse, C., de Wolf, H., Cohen, K.M., 2005.
 989 Sedimentary architecture and optical dating of Middle and Late Pleistocene Rhine-Meuse deposits
 990 — fluvial response to climate change, sea-level fluctuation and glaciation. *Netherlands Journal of*
 991 *Geosciences* 84, 25–41.

992 Campo, B., Amorosi, A., Bruno, L., 2016. Contrasting alluvial architecture of Late Pleistocene and
 993 Holocene deposits along a 120-km transect from the central Po Plain (northern Italy). *Sediment.*
 994 *Geol.* 341, 265–275.

995 Campo, B., Amorosi, A., Vaiani, S.C., 2017. Sequence stratigraphy and late Quaternary
 996 paleoenvironmental evolution of the Northern Adriatic coastal plain (Italy). *Palaeogeogr.*
 997 *Palaeoclimatol. Palaeoecol.* 466, 265–278.

998 Carruba, S., Casnedi, R., Perotti, C.R., Tornaghi, M., Bolis, G., 2006. Tectonic and sedimentary evolution
 999 of the lower Pliocene Periadriatic foredeep in Central Italy. *Int. J. Earth Sci.* 95, 665–683.
 1000 <https://doi.org/10.1007/s00531-005-0056-4>

1001 Cattaneo, A., Steel, R.J., 2003. Transgressive deposits: an overview of their variability. *Earth—Science*
 1002 *Reviews* 62, 187–228.

1003 Cattaneo, A., Trincardi, F., 1999. The Late-Quaternary transgressive record in the Adriatic epicontinental
 1004 sea: basin widening and facies partitioning. In: Bergman, K.M., Snedden, J.W., (Eds.), *Isolated*
 1005 *Shallow Marine Sand Bodies: Sequence Stratigraphic Analysis and Sedimentologic Interpretation.*
 1006 *SEPM Special Publication* 64, pp. 127–146.

1007 Cattaneo, A., Trincardi, F., Asioli, A., Correggiari, A., 2007. The Western Adriatic shelf clinoform: energy-
1008 limited bottomset. *Cont. Shelf Res.* 27, 506–525. <https://doi.org/10.1016/j.csr.2006.11.013>

1009 Catuneanu, O., 2019. Scale in sequence stratigraphy. *Mar. Pet. Geol.* 106, 128–159.
1010 <https://doi.org/10.1016/j.marpetgeo.2019.04.026>

1011 Catuneanu, O., 2006. Principles of sequence stratigraphy, Elsevier, Amsterdam, 386 pp.
1012 <https://doi.org/10.5860/choice.44-4462>

1013 Catuneanu, O., Abreu, V., Bhattacharya, J.P., Blum, M.D., Dalrymple, R.W., Eriksson, P.G., Fielding,
1014 C.R., Fisher, W.L., Galloway, W.E., Gibling, M.R., Giles, K.A., Holbrook, J.M., Jordan, R.,
1015 Kendall, C.G.S.C., Macurda, B., Martinsen, O.J., Miall, A.D., Neal, J.E., Nummedal, D., Pomar,
1016 L., Posamentier, H.W., Pratt, B.R., Sarg, J.F., Shanley, K.W., Steel, R.J., Strasser, A., Tucker, M.E.,
1017 Winker, C., 2009. Towards the standardization of sequence stratigraphy. *Earth-Science Rev.* 92,
1018 1–33. <https://doi.org/10.1016/j.earscirev.2008.10.003>

1019 Chaumillon, E., Tessier, B., Reynaud, J.Y., 2010. Stratigraphic records and variability of Incised valleys
1020 and estuaries along French coasts. *Bull. la Soc. Geol. Fr.* 181, 75–85.
1021 <https://doi.org/10.2113/gssgfbull.181.2.75>

1022 Cheng, H., Zhang, H., Spötl, C., Baker, J., Sinha, A., Li, H., Bartolomé, M., Moreno, A., Kathayat, G.,
1023 Zhao, J., Dong, X., Li, Y., Ning, Y., Jia, X., Zong, B., Brahim, Y.A., Pérez-Mejías, C., Cai, Y.,
1024 Novello, V.F., Cruz, F.W., Severinghaus, J.P., An, Z., Edwards, R.L., 2020. Timing and structure
1025 of the Younger Dryas event and its underlying climate dynamics. *Proc. Natl. Acad. Sci. U. S. A.*
1026 117, 23408–23417. <https://doi.org/10.1073/pnas.2007869117>

1027 Chua, S., Switzer, A.D., Kearsey, T.I., Bird, M.I., Rowe, C., Chiam, K., Horton, B.P., 2020. A new
1028 Quaternary stratigraphy of the Kallang River Basin, Singapore: Implications for urban development
1029 and geotechnical engineering in Singapore. *J. Asian Earth Sci.* 200, 104430.

1030 Cilumbriello, A., Sabato, L., Tropeano, M., Gallicchio, S., Grippa, A., Maiorano, P., Mateu-Vicens, G.,
1031 Rossi, C.A., Spilotro, G., Calcagnile, L., Quarta, G., 2010. Sedimentology, stratigraphic
1032 architecture and preliminary hydrostratigraphy of the Metaponto coastal-plain subsurface

1033 (Southern Italy), in: Bersezio, R., Amanti, M. (Eds.), Proceedings of the National Workshop
 1034 “Multidisciplinary Approach for Porous Aquifer Characterization”. Mem. Descr. Carta Geol. d’it.,
 1035 pp. 75–92.

1036 Clark, P.U., Dyke, A.S., Shakun, J.D., Carlson, A.E., Clark, J., Wohlfarth, B., Mitrovica, J.X., Hostetler,
 1037 S.W., McCabe, A.M., 2009. The Last Glacial Maximum. *Science* 325, 710–714.
 1038 <https://doi.org/10.1126/science.1172873>

1039 Coccioni, R., 2000. Benthic foraminifera as bioindicators of heavy metal pollution—A case study from the
 1040 Goro Lagoon (Italy), in: Martin, R.E., (Ed.), *Environmental Micropaleontology: The Application*
 1041 *of Microfossils to Environmental Geology*, Kluwer Academic/Plenum Publishers, New York, pp.
 1042 71–103.

1043 Correggiari, A., Roveri, M., Trincardi, F., 1996. Late pleistocene and holocene evolution of the North
 1044 Adriatic Sea. *Alp. Mediterr. Quat.* 9, 697–704.

1045 Crescenti, U., D’amato, C., 1980. Il Plio-Pleistocene del sottosuolo abruzzese-marchigiano tra Ascoli
 1046 Piceno e Pescara.

1047 Cross, T.A., Baker, M.R., Chapin, M.A., Clark, M.S., Gardner, M.H., Hanson, M.S., Lessenger, M.A.,
 1048 Little, L.D., McDonough, K.J., Sonnenfield, M.D., Valasek, D.W., Williams, M.R., Witter, D.N.,
 1049 1993. Applications of high-resolution sequence stratigraphy to reservoir analysis, in: Eschard, R.,
 1050 Doligez, B. (Eds.), *Subsurface Reservoir Characterization from Outcrop Observations. Proceedings*
 1051 *7th IFP Exploration and Production Conference*, pp. 11–33.

1052 D’Alessandro, L., Genevois, R., Marino, A., 2001. Dinamica recente della costa alta tra Ortona e Vasto
 1053 (Abruzzo centro meridionale). *Mem. della Soc. Geol. Ital.* 56, 53–60.

1054 D’Alessandro, L., Miccadei, E., Piacentini, T., 2008. Morphotectonic study of the lower Sangro River
 1055 valley (Abruzzi, Central Italy). *Geomorphology* 102, 145–158.
 1056 <https://doi.org/10.1016/j.geomorph.2007.06.019>

1057 D’Alessandro, L., Miccadei, E., Piacentini, T., 2003. Morphostructural elements of central-eastern Abruzzi:

1058 Contributions to the study of the role of tectonics on the morphogenesis of the Apennine chain.
 1059 Quat. Int. 101–102, 115–124. [https://doi.org/10.1016/S1040-6182\(02\)00094-0](https://doi.org/10.1016/S1040-6182(02)00094-0)

1060 D’Amico, C., Aiello, G., Barra, D., Bracone, V., Di Bella, L., Esu, D., Frezza, V., Rosskopf, C.M., 2013.
 1061 Late quaternary foraminiferal, molluscan and ostracod assemblages from a core succession in the
 1062 Trigno River mouth area (Central Adriatic sea, Italy). Boll. della Soc. Paleontol. Ital. 52, 197–205.
 1063 <https://doi.org/10.4435/BSPI.2013.23>

1064 Dalla, S., Harby, H., Serazzi, M., 1997. Hydrocarbon exploration in a complex incised valley fill: an
 1065 example from the late Messinian Abu Madi Formation (Nile Delta Basin, Egypt). Lead. Edge 16,
 1066 1819–1826.

1067 Dalla Valle, G., Gamberi, F., Rocchini, P., Minisini, D., Errera, A., Baglioni, L., Trincardi, F., 2013b. 3D
 1068 seismic geomorphology of mass transport complexes in a foredeep basin: examples from the
 1069 Pleistocene of the Central Adriatic Basin (Mediterranean Sea). Sediment. Geol. 294, 126–141.

1070 Dalla Valle, G., Gamberi, F., Trincardi, F., Rocchini, P., Errera, A., Baglioni, L., 2013a. Contrasting slope
 1071 channel styles on a prograding mud-prone margin. Mar. Pet. Geol. 41, 72–82.

1072 Dalrymple, R.W., Boyd, R., Zaitlin, B.A., 1994. Incised-valley systems: origin and sedimentary sequences.
 1073 SEPM Special Publication, 51.

1074 Dalrymple, R.W., Leckie, D.A., Tillman, R.W., 2006. Incised Valleys in Time and Space: SEPM Special
 1075 Publication, 85.

1076 Dalrymple, R.W., Zaitlin, B.A., Boyd, R., 1992. Estuarine facies models: conceptual basis and stratigraphic
 1077 implications. J. Sediment. Petrol. 62, 1130–1146.

1078 Debenay, J.P., Guillou, J.J., Redois, F., Geslin, E., 2000. Distribution trends of foraminiferal assemblages
 1079 in paralic environments: a base for using foraminifera as bioindicators, in: Martin, R.E., (Ed.),
 1080 Environmental Micropaleontology: The Application of Microfossils to Environmental Geology,
 1081 Kluwer Academic/Plenum Publishers, New York, pp. 39–67.

1082 De Santis, V., Caldara, M., 2016. Evolution of an incised valley system in the southern Adriatic Sea

1083 (Apulian margin): an onshore–offshore correlation. *Geol. J.* 51, 263–284.

1084 De Santis, V., Caldara, M., Pennetta, L., 2020a. “Continuous” backstepping of Holocene coastal barrier
 1085 systems into incised valleys: Insights from the Ofanto and Carapelle-Cervaro valleys. *Water*
 1086 (Switzerland) 12. <https://doi.org/10.3390/w12061799>

1087 De Santis, V., Caldara, M., Pennetta, L., 2020b. Transgressive architecture of coastal barrier systems in the
 1088 ofanto incised valley and its surrounding shelf in response to stepped sea-level rise. *Geosci.* 10, 1–
 1089 27. <https://doi.org/10.3390/geosciences10120497>

1090 Della Seta, M., Del Monte, M., Fredi, P., Miccadei, E., Nesci, O., Pambianchi, G., Piacentini, T., Troiani,
 1091 F., 2008. Morphotectonic evolution of the Adriatic piedmont of the Apennines: An advancement
 1092 in the knowledge of the Marche-Abruzzo border area. *Geomorphology* 102, 119–129.
 1093 <https://doi.org/10.1016/j.geomorph.2007.06.018>

1094 Denton, G.H., Anderson, R.F., Toggweiler, J.R., Edwards, R.L., Schaefer, J.M., Putnam, A.E., 2010. The
 1095 last glacial termination. *Science* 328, 1652–1656. <https://doi.org/10.1126/science.1184119>

1096 Desiderio, G., Ferracuti, L., Rusi, S., 2007. Structural-stratigraphic setting of middle Adriatic alluvial plains
 1097 and its control on quantitative and qualitative groundwater circulation, in: *Mem. Descr. Carta Geol.*
 1098 *d’it.*, pp. 147–162.

1099 Drago, T., Freitas, C., Rocha, F., Moreno, J., Cachão, M., Naughton, F., Fradique, C., Araújo, F., Silveira,
 1100 T., Oliveira, A., 2006. Paleoenvironmental evolution of estuarine systems during the last 14000
 1101 years-the case of Douro estuary (NW Portugal). *J. Coast. Res.* 186–192.

1102 Durand, M., Mojtahid, M., Maillet, G.M., Baltzer, A., Schmidt, S., Blet, S., Marchès, E., Howa, H., 2018.
 1103 Late Holocene record from a Loire River incised paleovalley (French inner continental shelf):
 1104 Insights into regional and global forcing factors. *Palaeogeogr. Palaeoclimatol. Palaeoecol.* 511, 12–
 1105 28. <https://doi.org/10.1016/j.palaeo.2018.06.035>

1106 Ellis, B.F., Messina, A.R., 1940. *Catalogue of Foraminifera*; Micropaleontology Press, New York, NY,
 1107 USA.

1108 Ellis, B.F., Messina, A.R., 1952. Catalogue of Ostracoda. The American Museum of Natural History
 1109 Special Publications, New York, NY, USA.

1110 Fairbanks, R.G., 1989. A 17,000-year glacio-eustatic sea level record: influence of glacial melting rates on
 1111 the Younger Dryas event and deep-ocean circulation. *Nature* 342, 637–642.

1112 Forzoni, A., Storms, J.E.A., Reimann, T., Moreau, J., Jouet, G., 2015. Non-linear response of the Golo
 1113 River system, Corsica, France, to Late Quaternary climatic and sea level variations. *Quat. Sci. Rev.*
 1114 121, 11–27. <https://doi.org/10.1016/j.quascirev.2015.04.021>

1115 Gamberi, F., Pellegrini, C., Dalla Valle, G., Scarponi, D., Bohacs, K., Trincardi, F., 2020. Compound and
 1116 hybrid clinothems of the last lowstand Mid-Adriatic Deep: Processes, depositional environments,
 1117 controls and implications for stratigraphic analysis of prograding systems. *Basin Res.* 32, 363–377.
 1118 <https://doi.org/10.1111/bre.12417>

1119 Geological Map of Italian Seas at 1:250,000 scale (Geological Survey of Italy and CARG Project), Sheet:
 1120 NK-33-5 Pescara
 1121 https://www.isprambiente.gov.it/Media/carg/marine/NK_33_5_PESCARA_SOTT/Foglio.html

1122 Geological Map of Italy at 1:50,000 scale (Geological Survey of Italy and CARG Project), Sheet: 351.
 1123 https://www.isprambiente.gov.it/Media/carg/note_illustrative/351_Pescara.pdf

1124 Geological Map of Italy at 1:50,000 scale (Geological Survey of Italy and CARG Project), Sheet: 361.
 1125 https://www.isprambiente.gov.it/Media/carg/note_illustrative/361_Chieti.pdf

1126 Gibling, M.R., Bird, D.J., 1994. Late Carboniferous cyclothems and alluvial paleovalleys in the Sydney
 1127 Basin, Nova Scotia. *Geol. Soc. Am Bull.* 106(1), 105-117.

1128 Gibling, M.R., Fielding, C.R., Sinha, R., Davidson, S.K., Leleu, S., North, C.P., 2011. Alluvial valleys and
 1129 alluvial sequences: towards a geomorphic assessment. *From River to Rock Rec. Preserv. Fluv.*
 1130 *Sediments Their Subseq. Interpret.* SEPM Spec. Publ. 97, 423–447.

1131 Goetz, A.M., Beckie, R.D., Cahill, A.G., 2021. Groundwater recharge in a confined paleovalley setting,
 1132 Northeast British Columbia, Canada. *Hydrogeol. J.* 29, 1797–1812.

- 1133 Grano, M., Di Giuseppe, R., 2021. I molluschi terrestri e dulciacquicoli (Mollusca : Gastropoda , Bivalvia
1134) di Castel di Guido (Lazio , Italia centrale). Boll. Mus. reg. Sci. nat. Torino 38, 149–168.
- 1135 Grippa, A., Bianca, M., Tropeano, M., Cilumbriello, A., Gallipoli, M.R., Mucciarelli, M., Sabato, L., 2011.
1136 Use of the HVSR method to detect buried paleomorphologies (filled incised-valleys) below a
1137 coastal plain: The case of the metaponto plain (Basilicata, Southern Italy). Boll. di Geofis. Teor. ed
1138 Appl. 52, 1–16. <https://doi.org/10.4430/bgta0011>
- 1139 Guijia, Z. and Congxian, L., 1996. The fills and stratigraphic sequences in the Qiantangjiang incised
1140 paleovalley, China. J. Sediment. Res. 66(2), 406–414.
- 1141 Hampson, G., Stollhofen, H., Flint, S., 1999. A sequence stratigraphic model for the Lower Coal Measures
1142 (Upper Carboniferous) of the Ruhr district, north-west Germany. Sedimentology 46, 1199–1231.
1143 <https://doi.org/10.1046/j.1365-3091.1999.00273.x>
- 1144 Hanebuth, T.J.J., Stattegger, K., 2004. Depositional sequences on a late Pleistocene–Holocene tropical
1145 siliciclastic shelf (Sunda Shelf, southeast Asia). J. Asian Earth Sci. 23, 113–126.
- 1146 Harms, J.C., 1966. Stratigraphic Traps in a Valley Fill, Western Nebraska: ABSTRACT. Am. Assoc. Pet.
1147 Geol. Bull. 50, 2119–2149. <https://doi.org/10.1306/a663379c-16c0-11d7-8645000102c1865d>
- 1148 Harrison, S., Smith, D.E., Glasser, N.F., 2019. Late Quaternary meltwater pulses and sea level change. J.
1149 Quat. Sci. 34, 1–15.
- 1150 Henderson, P.A., 1990. Freshwater Ostracods, in: Kermack, D.M., Barnes, R.S.K., (Eds.), Synopses of the
1151 British Fauna (New Series), Leiden, The Netherlands, 228 p.
- 1152 Hickin, A.S., Best, M.E., 2013. Mapping the geometry and lithostratigraphy of a paleovalley with a time-
1153 domain electromagnetic technique in an area with small resistivity contrasts, Groundbirch, British
1154 Columbia, Canada. J. Environ. Eng. Geophys. 18, 119–135.
- 1155 Hijma, M.P., Cohen, K.M., Hoffmann, G., Van der Spek, A.J.F., Stouthamer, E., 2009. From river valley
1156 to estuary: the evolution of the Rhine river mouth in the early to middle Holocene (western
1157 Netherlands, Rhine-Meuse delta). Neth. J. Geosci. 88, 13–53.

1158 Hori, K., Saito, Y., Zhao, Q., Wang, P., 2002. Evolution of the coastal depositional systems of the
 1159 Changjiang (Yangtze) in response to late Pleistocene-Holocene sea-level changes. *J. Sediment.*
 1160 *Res.* 72, 884-897.

1161 Hori, K., Tanabe, S., Saito, Y., Haruyama, S., Nguyen, V., Kitamura, A., 2004. Delta initiation and
 1162 Holocene sea-level change: example from the Song Hong (Red River) delta, Vietnam. *Sediment.*
 1163 *Geol.* 164, 237–249.

1164 Horozal, S., Chae, S., Seo, J.M., Lee, S.M., Han, H.S., Cukur, D., Kim, E.D., Son, J.H., 2021. Quaternary
 1165 evolution of the southeastern Korean continental shelf, East Sea: Paleo-incised valley and channel
 1166 systems. *Mar. Pet. Geol.* 128, 105011. <https://doi.org/10.1016/j.marpetgeo.2021.105011>

1167 Ishihara, T., Sugai, T., 2017. Eustatic and regional tectonic controls on late Pleistocene paleovalley
 1168 morphology in the central Kanto Plain, Japan. *Quat. Int.* 456, 69–84.

1169 Jennette, D.C., Jones, C.R., Van Wagoner, J.C., Larsen, J.E., 1991. High-resolution sequence stratigraphy
 1170 of the Upper Cretaceous Tocito Sandstone: the relationship between incised valleys and
 1171 hydrocarbon accumulation, San Juan Basin, New Mexico, in: J.C. Van Wagoner, C.R. Jones, D.R.
 1172 Taylor, D. Nummedal, D.C. Jennette, G.W. Riley (Eds.), *Sequence stratigraphy applications to*
 1173 *shelf sandstone reservoirs, outcrop to subsurface examples*, 24-62.

1174 Jessen, S., Larsen, F., Postma, D., Viet, P.H., Ha, N.T., Nhan, P.Q., Nhan, D.D., Duc, M.T., Hue, N.T.M.,
 1175 Huy, T.D., 2008. Palaeo-hydrogeological control on groundwater As levels in Red River delta,
 1176 Vietnam. *Appl. Geochemistry* 23, 3116–3126.

1177 Jorissen, F.J., Barmawidjaja, D.M., Puskaric, S., Van der Zwaan, G.J., 1992. Vertical distribution of benthic
 1178 foraminifera in the northern Adriatic Sea: the relation with the organic flux. *Marine*
 1179 *Micropaleontol.* 19, 131-146.

1180 Kettner, A.J., Syvitski, J.P.M., 2008. Predicting discharge and sediment flux of the Po River, Italy since the
 1181 Last Glacial Maximum. In: de Boer, P.L. (Ed.), *Analogue and Numerical Forward Modeling of*
 1182 *Sedimentary Systems; From Understanding to Prediction: IAS Special Publication*, 40, pp. 171–
 1183 190.

- 1184 Kroonenberg, S.B., Alekseevski, N.I., Aliyeva, E., Allen, M.B., Aybulatov, D.N., Baba-Zadeh, A.,
1185 Badyukova, E.N., Davies, C.E., Hinds, D.J., Hoogendoorn, R.M., Huseynov, D., Ibrahimov, B.,
1186 Mamedov, P., Overeem, I., Rusakov, G. V., Suleymanova, S., Svitoch, A.A., Vincent, S.J., 2005.
1187 Two Deltas, Two Basins, One River, One Sea: The Modern Volga Delta as an Analogue of the
1188 Neogene Productive Series, South Caspian Basin, in: Giosan, L., Bhattacharya, J.P. (Eds.), *River*
1189 *Deltas—Concepts, Models, and Examples*. SEPM Society for Sedimentary Geology, pp. 231–256.
1190 <https://doi.org/10.2110/pec.05.83.0231>
- 1191 Lambeck, K., Antonioli, F., Anzidei, M., Ferranti, L., Leoni, G., Scicchitano, G., Silenzi, S., 2011. Sea
1192 level change along the Italian coast during the Holocene and projections for the future. *Quat. Int.*
1193 232, 250–257. <https://doi.org/10.1016/j.quaint.2010.04.026>
- 1194 Lambeck, K., Rouby, H., Purcell, A., Sun, Y., Sambridge, M., 2014. Sea level and global ice volumes from
1195 the Last Glacial Maximum to the Holocene. *Proc. Natl. Acad. Sci.* 111, 15296–15303.
- 1196 Legarreta, L., Uliana, M.A., 1998. Anatomy of hinterland depositional sequences: Upper Cretaceous fluvial
1197 strata, Neuquen Basin, west-central Argentina, in: Shanley, K.W., McCabe, P.J. (Eds.), *Relative*
1198 *Role of Eustasy, Climate and Tectonism in Continental Rocks*. SEPM Special Publication, pp. 83–
1199 92.
- 1200 Leithold, E.L., Blair, N.E., Wegmann, K.W., 2016. Source-to-sink sedimentary systems and global carbon
1201 burial: A river runs through it. *Earth-Science Rev.* 153, 30–42.
- 1202 Liu, H., Meng, J., Zhang, Y., Yang, L., 2019. Pliocene seismic stratigraphy and deep-water sedimentation
1203 in the Qiongdongnan Basin, South China Sea: Source-to-sink systems and hydrocarbon
1204 accumulation significance. *Geol. J.* 54, 392–408.
- 1205 Liu, J.P., Milliman, J.D., 2004. Reconsidering melt-water pulses 1A and 1B: Global impacts of rapid sea-
1206 level rise. *J. Ocean Univ. China* 3, 183–190. <https://doi.org/10.1007/s11802-004-0033-8>
- 1207 Liu, J.P., Milliman, J.D., Gao, S., Cheng, P., 2004. Holocene development of the Yellow River's
1208 subaqueous delta, North Yellow Sea. *Mar. Geol.* 209, 45–67.
1209 <https://doi.org/10.1016/j.margeo.2004.06.009>

1210 Lowe, J.J., Blockley, S., Trincardi, F., Asioli, A., Cattaneo, A., Matthews, I.P., Pollard, M., Wulf, S., 2007.
 1211 Age modelling of late Quaternary marine sequences in the Adriatic: towards improved precision
 1212 and accuracy using volcanic event stratigraphy. *Cont. Shelf Res.* 27, 560–582.

1213 Macklin, M.G., Fuller, I.C., Lewin, J., Maas, G.S., Passmore, D.J., Rose, J., Woodward, J.C., Black, S.,
 1214 Hamlin, R.H.B., Rowan, J.S., 2002. Correlation of fluvial sequences in the Mediterranean basin
 1215 over the last 200 ka and their relationship to climate change. *Quat. Sci. Rev.* 21, 1633–1641.

1216 Maselli, V., Hutton, E.W., Kettner, A.J., Syvitski, J.P.M., Trincardi, F., 2011. High-frequency sea level and
 1217 sediment supply fluctuations during Termination I: An integrated sequence-stratigraphy and
 1218 modeling approach from the Adriatic Sea (Central Mediterranean). *Mar. Geol.* 287, 54–70.
 1219 <https://doi.org/10.1016/j.margeo.2011.06.012>

1220 Maselli, V., Trincardi, F., 2013. Large-scale single incised valley from a small catchment basin on the
 1221 western Adriatic margin (central Mediterranean Sea). *Glob. Planet. Change* 100, 245–262.
 1222 <https://doi.org/10.1016/j.gloplacha.2012.10.008>

1223 Maselli, V., Trincardi, F., Asioli, A., Ceregato, A., Rizzetto, F., Taviani, M., 2014. Delta growth and river
 1224 valleys: The influence of climate and sea level changes on the South Adriatic shelf (Mediterranean
 1225 Sea). *Quat. Sci. Rev.* 99, 146–163. <https://doi.org/10.1016/j.quascirev.2014.06.014>

1226 Maselli, V., Trincardi, F., Cattaneo, A., Ridente, D., Asioli, A., 2010. Subsidence pattern in the central
 1227 Adriatic and its influence on sediment architecture during the last 400 kyr. *J. Geophys. Res. Solid*
 1228 *Earth* 115, 1–23. <https://doi.org/10.1029/2010JB007687>

1229 Matheus, C.R., Rodriguez, A.B., 2014. Controls on lower-coastal-plain valley morphology and fill
 1230 architecture. *J. Sediment. Res.* 84, 314–325. <https://doi.org/10.2110/jsr.2014.30>

1231 McGhee, C., Muhammed, D., Simon, N., Acikalin, S., Utley, J.E.P., Griffiths, J., Wooldridge, L., Verhagen,
 1232 I.T.E., van der Land, C., Worden, R.H., 2022. Stratigraphy and sedimentary evolution of a modern
 1233 macro-tidal incised valley: An analogue for reservoir facies and architecture. *Sedimentology* 69,
 1234 696–723. <https://doi.org/10.1111/sed.12922>

- 1235 Meisch, C., 2000. Freshwater Ostracoda of Western and Central Europe, Heidelberg, Spektrum, 522 p.
- 1236 Miall, A.D., 1992. Alluvial deposits, in: Walker, R.G., James, N.P. (Eds.), Facies Models: Response to Sea
1237 Level Change. Geological Association of Canada, Waterloo, Ontario, pp. 119-139.
- 1238 Milker, Y., Schmiedl, G., 2012. A taxonomic guide to modern benthic shelf foraminifera of the western
1239 Mediterranean Sea, *Palaeontologia Electronica* 15 (2), 16A, 134 p.
- 1240 Milli, S., D'Ambrogio, C., Bellotti, P., Calderoni, G., Carboni, M.G., Celant, A., Di Bella, L., Di Rita, F.,
1241 Frezza, V., Magri, D., Pichezzi, R.M., Ricci, V., 2013. The transition from wave-dominated estuary
1242 to wave-dominated delta: The Late Quaternary stratigraphic architecture of Tiber River deltaic
1243 succession (Italy). *Sediment. Geol.* 284–285, 159–180.
1244 <https://doi.org/10.1016/j.sedgeo.2012.12.003>
- 1245 Milli, S., Mancini, M., Moscatelli, M., Stigliano, F., Marini, M., Cavinato, G.P., 2016. From river to shelf,
1246 anatomy of a high-frequency depositional sequence: The Late Pleistocene to Holocene Tiber
1247 depositional sequence. *Sedimentology* 63, 1886–1928. <https://doi.org/10.1111/sed.12277>
- 1248 Neal, J.E., Abreu, V., 2009. Sequence stratigraphy hierarchy and the accommodation succession method.
1249 *Geology* 37, 779–782. <https://doi.org/10.1130/G25722A.1>
- 1250 Neal, J.E., Abreu, V., Bohacs, K.M., Feldman, H.R., Pederson, K.H., 2016. Accommodation succession
1251 ($\delta A/\delta S$) sequence stratigraphy: Observational method, utility and insights into sequence boundary
1252 formation. *J. Geol. Soc. London.* 173, 803–816. <https://doi.org/10.1144/jgs2015-165>
- 1253 Ori, G.G., Roveri, M., Vannoni, F., 1986. Plio-Pleistocene sedimentation in the Apenninic foredeep
1254 (Central Adriatic Sea, Italy), in: Allen, P.A., Homewood, P. (Eds.), *Foreland Basins*. IAS Special
1255 Publication 8, pp. 183-198.
- 1256 Ori, G.G., Serafini, G., Visentin, F., Ricci Lucchi, F., Casnedi, R., Colalongo, M.L., Mosna, S., 1991. The
1257 Pliocene end Pleistocene Adriatic foredeep (Marche and Abruzzo, Italy): an integrated approach
1258 to surface and subsurface geology, in: *Third Conference of the European Association of
1259 Petroleum Geology*, May 1991, Adriatic Foredeep Field Trip Guide Book, 85, Florence, Italy.

1260 Parlagreco, L., Mascioli, F., Miccadei, E., Antonioli, F., Gianolla, D., Devoti, S., Leoni, G., Silenzi, S.,
 1261 2011. New data on Holocene relative sea level along the Abruzzo coast (central Adriatic, Italy).
 1262 Quat. Int. 232, 179–186. <https://doi.org/10.1016/j.quaint.2010.07.021>

1263 Pasini, G., Colalongo, M., 1996. The Pliocene–Pleistocene boundary-stratotype at Vrica, Italy, in:
 1264 Couvring, J., (Ed.), The Pleistocene Boundary and the Beginning of the Quaternary, World and
 1265 Regional Geology, Cambridge: Cambridge University Press. pp. 15–45.
 1266 doi:10.1017/CBO9780511585760.004

1267 Payenberg, T.H.D., Boyd, R., Beaudoin, J., Ruming, K., Davies, S., Roberts, J., Lang, S.C., 2006. The
 1268 Filling of an Incised Valley by Shelf Dunes—an example from Hervey Bay, East Coast OF
 1269 Australia, in: Dalrymple, R.W., Leckie, D.A., Tillman, R.. (Eds.), Incised Valleys in Time and
 1270 Space. SEPM Special Publication, pp. 87–98. <https://doi.org/10.2110/pec.06.85.0087>

1271 Peeters, J., Busschers, F.S., Stouthamer, E., 2015. Fluvial evolution of the Rhine during the last interglacial-
 1272 glacial cycle in the southern North Sea basin: A review and look forward. Quat. Int. 357, 176–188.
 1273 <https://doi.org/10.1016/j.quaint.2014.03.024>

1274 Pellegrini, C., Asioli, A., Bohacs, K.M., Drexler, T.M., Feldman, H.R., Sweet, M.L., Maselli, V., Rovere,
 1275 M., Gamberi, F., Valle, G.D., Trincardi, F., 2018. The late Pleistocene Po River lowstand wedge
 1276 in the Adriatic Sea: Controls on architecture variability and sediment partitioning. Mar. Pet. Geol.
 1277 96, 16–50. <https://doi.org/10.1016/j.marpetgeo.2018.03.002>

1278 Pellegrini, C., Tesi, T., Schieber, J., Bohacs, K.M., Rovere, M., Asioli, A., Nogarotto, A., Trincardi, F.,
 1279 2021. Fate of terrigenous organic carbon in muddy clinothems on continental shelves revealed by
 1280 stratal geometries: Insight from the Adriatic sedimentary archive. Glob. Planet. Change 203,
 1281 103539. <https://doi.org/10.1016/j.gloplacha.2021.103539>

1282 Pellegrini, C., Maselli, V., Gamberi, F., Asioli, A., Bohacs, K.M., Drexler, T.M., Trincardi, F., 2017. How
 1283 to make a 350-m-thick lowstand systems tract in 17,000 years: The Late Pleistocene Po River (Italy)
 1284 lowstand wedge. Geology 45, 327–330. <https://doi.org/10.1130/G38848.1>

1285 Phillips, J.D., Slattery, M.C., Musselman, Z.A., 2004. Dam-to-delta sediment inputs and storage in the

1286 lower trinity river, Texas. *Geomorphology* 62, 17–34.
 1287 <https://doi.org/10.1016/j.geomorph.2004.02.004>

1288 Pillans, B., Gibbard, P., 2012. The quaternary period, in: *The Geologic Time Scale 2012*. Elsevier.

1289 Pint, A., Frenzel, P., 2017. Ostracod Fauna Associated with *Cyprideis torosa* - An Overview. *J.*
 1290 *Micropalaeontol.*, 36, pp. 113–119.

1291 Piva, A., Asioli, A., Andersen, N., Grimalt, J.O., Schneider, R.R., Trincardi, F., 2008a. Climatic cycles as
 1292 expressed in sediments of the PROMESS1 borehole PRAD1-2, central Adriatic, for the last 370
 1293 ka: 2. Paleoenvironmental evolution. *Geochemistry, Geophys. Geosystems* 9.
 1294 <https://doi.org/10.1029/2007GC001785>

1295 Piva, A., Asioli, A., Schneider, R.R., Trincardi, F., Andersen, N., Colmenero-Hidalgo, E., Dennielou, B.,
 1296 Flores, J.A., Vigliotti, L., 2008b. Climatic cycles as expressed in sediments of the PROMESSI
 1297 borehole PRAD1-2, central Adriatic, for the last 370 ka: 1. Integrated stratigraphy. *Geochemistry,*
 1298 *Geophys. Geosystems* 9. <https://doi.org/10.1029/2007GC001713>

1299 Plint, A.G., Nummedal, D., 2000. The falling stage systems tract: recognition and importance in sequence
 1300 stratigraphic analysis, in: Hunt, D., Gawthorpe, R.L., (Eds.), *Sedimentary Responses to Forced*
 1301 *Regressions: Geol. Soc. London Special Publications*, 172, pp. 1-17.

1302 Posamentier, H.W., Jervey, M.T., Vail, P.R., 1988. Eustatic controls on clastic deposition I—conceptual
 1303 framework, in: Wilgus, C.K., Hastings, B.S., Kendal, C.G.C., Posamentier, H.W., Ross, C.A., Van
 1304 Wagoner, J.C. (Eds.), *Sea-Level Changes: An Integrated Approach*. *SEPM Special Publication*, 42,
 1305 pp. 109–124.

1306 Ramsey, C.B., 1995. Radiocarbon Calibration and Analysis of Stratigraphy: The OxCal Program.
 1307 *Radiocarbon* 37, 425–430. <https://doi.org/10.1017/S0033822200030903>

1308 Ramsey, C.B., Lee, S., 2013. Recent and Planned Developments of the Program OxCal. *Radiocarbon* 55,
 1309 720–730. <https://doi.org/10.1017/s0033822200057878>

- Rasmussen, T.L., 2005. Systematic paleontology and ecology of benthic foraminifera from the Plio-Pleistocene Kallithea Bay Section, Rhodes, Greece, in: Rasmussen, T.L., Hastrup, A., Thomsen, E., (Eds.), Lagoon to Deep-water Foraminifera and Ostracods From the Plio-Pleistocene Kallithea Bay Section, Rhodes, Greece Special Publication 39. Cushman Foundation, Fredericksburg, Virginia, pp. 53–157.
- Reimer, P.J., Austin, W.E.N., Bard, E., Bayliss, A., Blackwell, P.G., Bronk Ramsey, C., Butzin, M., Cheng, H., Edwards, R.L., Friedrich, M., Grootes, P.M., Guilderson, T.P., Hajdas, I., Heaton, T.J., Hogg, A.G., Hughen, K.A., Kromer, B., Manning, S.W., Muscheler, R., Palmer, J.G., Pearson, C., Van Der Plicht, J., Reimer, R.W., Richards, D.A., Scott, E.M., Southon, J.R., Turney, C.S.M., Wacker, L., Adolphi, F., Büntgen, U., Capano, M., Fahrni, S.M., Fogtmann-Schulz, A., Friedrich, R., Köhler, P., Kudsk, S., Miyake, F., Olsen, J., Reinig, F., Sakamoto, M., Sookdeo, A., Talamo, S., 2020. The IntCal20 Northern Hemisphere Radiocarbon Age Calibration Curve (0-55 cal kBP). Radiocarbon 62, 725–757. <https://doi.org/10.1017/RDC.2020.41>
- Ridente, D., Trincardi, F., Piva, A., Asioli, A., Cattaneo, A., 2008. Sedimentary response to climate and sea level changes during the past ~400 ka from borehole PRAD1-2 (Adriatic margin). Geochemistry, Geophys. Geosystems 9. <https://doi.org/10.1029/2007GC001783>
- Rittenour, T.M., Blum, M.D., Goble, R.J., 2007. Fluvial evolution of the lower Mississippi River valley during the last 100 k.y. glacial cycle: Response to glaciation and sea-level change. Bull. Geol. Soc. Am. 119, 586–608. <https://doi.org/10.1130/B25934.1>
- Rodriguez, A.B., Anderson, J.B., Bradford, J., 1998. Holocene tidal deltas of the Trinity incised valley: analogs for exploration and production.
- Ronchi, L., Fontana, A., Cohen, K.M., Stouthamer, E., 2021. Late Quaternary landscape evolution of the buried incised valley of Concordia Sagittaria (Tagliamento River, NE Italy): A reconstruction of incision and transgression. Geomorphology 373, 107509. <https://doi.org/10.1016/j.geomorph.2020.107509>
- Ronchi, L., Fontana, A., Correggiari, A., Asioli, A., 2018. Late Quaternary incised and infilled landforms

1336 in the shelf of the northern Adriatic Sea (Italy). *Mar. Geol.* 405, 47–67.
 1337 <https://doi.org/10.1016/j.margeo.2018.08.004>

1338 Rossi, V., Amorosi, A., Sarti, G., Potenza, M., 2011. Influence of inherited topography on the Holocene
 1339 sedimentary evolution of coastal systems: an example from Arno coastal plain (Tuscany, Italy).
 1340 *Geomorphology* 135, 117–128.

1341 Rossi, V., Barbieri, G., Vaiani, S.C., Cacciari, M., Bruno, L., Campo, B., Marchesini, M., Marvelli, S.,
 1342 Amorosi, A., 2021. Millennial-scale shifts in microtidal ecosystems during the Holocene: dynamics
 1343 and drivers of change from the Po Plain coastal record (NE Italy). *J. Quat. Sci.* 36, 961–979.
 1344 <https://doi.org/10.1002/jqs.3322>

1345 Rossi, V., Vaiani, S.C., 2008. Benthic foraminiferal evidence of sediment supply changes and fluvial
 1346 drainage reorganization in Holocene deposits of the Po Delta, Italy. *Mar. Micropaleontol.* 69, 106–
 1347 118. <https://doi.org/10.1016/j.marmicro.2008.07.001>

1348 Ruberti, D., Sacchi, M., Pepe, F., Vigliotti, M., 2018. LGM incised valley in a volcanic setting. The northern
 1349 Campania Plain (Southern Italy). *Alp. Mediterr. Quat.* 31, 35–38.

1350 Salem, A.M., Ketzer, J.M., Morad, S., Rizk, R.R., Al-Aasm, I.S., 2005. Diagenesis and reservoir-quality
 1351 evolution of incised-valley sandstone: Evidence from the Abu Madi gas reservoirs (upper
 1352 Miocene), the Nile Delta Basin, Egypt. *J. Sediment. Res.* 75, 572–584.
 1353 <https://doi.org/10.2110/jsr.2005.047>

1354 Scarponi, D., Azzarone, M., Kowalewski, M., Huntley, J.W., 2017. Surges in trematode prevalence linked
 1355 to centennial-scale flooding events in the Adriatic. *Sci. Rep.* 7, 6–11.
 1356 <https://doi.org/10.1038/s41598-017-05979-6>

1357 Seifert, D., Sonnenborg, T.O., Scharling, P., Hinsby, K., 2008. Use of alternative conceptual models to
 1358 assess the impact of a buried valley on groundwater vulnerability. *Hydrogeol. J.* 16, 659–674.

1359 Shanley, K.W., McCabe, P.J., 1991. Predicting facies architecture through sequence stratigraphy - an
 1360 example from the Kaiparowits Plateau, Utah. *Geology* 19, 742–745. <https://doi.org/10.1130/0091->

[7613\(1991\)019<0742:PFATSS>2.3.CO;2](https://doi.org/10.1306/bdff9258-1718-11d7-8645000102c1865d)

- Shanley, K.W., McCabe, P.J., 1994. Perspectives on the sequence stratigraphy of continental strata: report of a working group at the 1991 NUNA Conference on High Resolution Sequence Stratigraphy. AAPG Bull. 78, 544-568. <https://doi.org/10.1306/bdff9258-1718-11d7-8645000102c1865d>
- Shanley, K.W., McCabe, P.J., Flint, S.S., Bryant, I.D., 1993. Alluvial architecture in a sequence stratigraphic framework: a case history from the Upper Cretaceous of southern Utah, USA, in: The Geological Modelling of Hydrocarbon Reservoirs and Outcrop Analogues. IAS Special Publication 15, pp. 21–55.
- Shaver, R.B., Pusc, S.W., 1992. Hydraulic barriers in Pleistocene buried-valley aquifers. Groundwater 30, 21–28.
- Simms, A.R., Aryal, N., Miller, L., Yokoyama, Y., 2010. The incised valley of Baffin Bay, Texas: A tale of two climates. Sedimentology 57, 642–669. <https://doi.org/10.1111/j.1365-3091.2009.01111.x>
- Smith, D.E., Harrison, S., Firth, C.R., Jordan, J.T., 2011. The early Holocene sea level rise. Quat. Sci. Rev. 30, 1846–1860. <https://doi.org/10.1016/j.quascirev.2011.04.019>
- Sømme, T.O., Piper, D.J.W., Deptuck, M.E., Helland-Hansen, W., 2011. Linking onshore-offshore sediment dispersal in the golo source-to-sink system (Corsica, France) during the late quaternary. J. Sediment. Res. 81, 118–137. <https://doi.org/10.2110/jsr.2011.11>
- Song, B., Yi, S., Yu, S.-Y., Nahm, W.-H., Lee, J.-Y., Lim, J., Kim, J.-C., Yang, Z., Han, M., Jo, K., 2018. Holocene relative sea-level changes inferred from multiple proxies on the west coast of South Korea. Palaeogeogr. Palaeoclimatol. Palaeoecol. 496, 268–281.
- Storms, J.E.A., Weltje, G.J., Terra, G.J., Cattaneo, A., Trincardi, F., 2008. Coastal dynamics under conditions of rapid sea-level rise: Late Pleistocene to Early Holocene evolution of barrier–lagoon systems on the northern Adriatic shelf (Italy). Quat. Sci. Rev. 27, 1107–1123.
- Sweet, M.L., Gaillot, G.T., Jouet, G., Rittenour, T.M., Toucanne, S., Marsset, T., Blum, M.D., 2020. Sediment routing from shelf to basin floor in the Quaternary Golo System of Eastern Corsica,

1386 France, western Mediterranean Sea. Bull. Geol. Soc. Am. 132, 1217–1234.
 1387 <https://doi.org/10.1130/B35181.1>

1388 Syvitski, J.P.M., Kettner, A.J., 2007. On the flux of water and sediment into the Northern Adriatic Sea.
 1389 Cont. Shelf Res. 27, 296–308.

1390 Ta, T.K.O., Nguyen, V.L., Saito, Y., Gugliotta, M., Tamura, T., Nguyen, T.M.L., Truong, M.H., Bui, T.L.,
 1391 2021. Latest Pleistocene to Holocene stratigraphic record and evolution of the Paleo-Mekong
 1392 incised valley, Vietnam. Mar. Geol. 433, 106406. <https://doi.org/10.1016/j.margeo.2020.106406>

1393 Tanabe, S., 2020. Stepwise accelerations in the rate of sea-level rise in the area north of Tokyo Bay during
 1394 the Early Holocene. Quat. Sci. Rev. 248, 106575. <https://doi.org/10.1016/j.quascirev.2020.106575>

1395 Tanabe, S., Saito, Y., Vu, Q.L., Hanebuth, T.J.J., Ngo, Q.L., Kitamura, A., 2006. Holocene evolution of
 1396 the Song Hong (Red River) delta system, northern Vietnam. Sediment. Geol. 187, 29–61.

1397 Tanabe, S., Ishihara, Y., Nakanishi, T., Stafleu, J., Busschers, F.S., 2021. Distribution of holocene marine
 1398 mud and its relation to damage from the 1923 earthquake disaster in the Tokyo metropolitan area,
 1399 Japan. Geosci. 11. <https://doi.org/10.3390/geosciences11070272>

1400 Tanabe, S., Nakanishi, T., Ishihara, Y., Nakashima, R., 2015. Millennial-scale stratigraphy of a tide-
 1401 dominated incised valley during the last 14 kyr: Spatial and quantitative reconstruction in the Tokyo
 1402 Lowland, central Japan. Sedimentology 62, 1837–1872. <https://doi.org/10.1111/sed.12204>

1403 Tanabe, S., Nakashima, R., Ishihara, Y., 2022. Transition from a transgressive to a regressive river-mouth
 1404 sediment body in Tokyo Bay during the early Holocene: Sedimentary facies, geometry, and
 1405 stacking pattern. Sediment. Geol. 428, 106059. <https://doi.org/10.1016/j.sedgeo.2021.106059>

1406 Tesi, T., Asioli, A., Minisini, D., Maselli, V., Valle, G.D., Gamberi, F., Langone, L., Cattaneo, A.,
 1407 Montagna, P., Trincardi, F., 2017. Large-scale response of the Eastern Mediterranean thermohaline
 1408 circulation to African monsoon intensification during sapropel S1 formation. Quat. Sci. Rev. 159,
 1409 139–154. <https://doi.org/10.1016/j.quascirev.2017.01.020>

1410 Thomas, M.A., Anderson, J.B., 1994. Sea-Level Controls on the Facies Architecture of the Trinity/Sabine

1411 Incised-Valley System, Texas Continental Shelf, in: Dalrymple, R.W., Boyd, R., Zaitlin, B.A.
 1412 (Eds.), Incised-Valley Systems: Origin and Sedimentary Sequences. SEPM Society for
 1413 Sedimentary Geology, pp. 63–82. <https://doi.org/10.2110/pec.94.12.0063>

1414 Tian, S.Y., Yasuhara, M., Hong, Y., Huang, H.-H.M., Iwatani, H., Chiu, W.-T.R., Mamo, B., Okahashi,
 1415 H., Rasmussen, T.L., 2020. Deglacial–Holocene Svalbard paleoceanography and evidence of
 1416 meltwater pulse 1B. *Quat. Sci. Rev.* 233, 106237.

1417 Trincardi, F., Cattaneo, A., Asioli, A., Correggiari, A., Langone, L., 1996. Stratigraphy of the late-
 1418 Quaternary deposits in the central Adriatic basin and the record of short-term climatic events. *Mem.*
 1419 *Ist. Ital. di Idrobiol.* 55, 39–70.

1420 Trincardi, F., Correggiari, A., Roveri, M., 1994. Late Quaternary transgressive erosion and deposition in a
 1421 modern epicontinental shelf: The Adriatic semienclosed basin. *Geo-Marine Lett.* 14, 41–51.
 1422 <https://doi.org/10.1007/BF01204470>

1423 Tropeano, M., Cilumbriello, A., Sabato, L., Gallicchio, S., Grippa, A., Longhitano, S.G., Bianca, M.,
 1424 Gallipoli, M.R., Mucciarelli, M., Spilotro, G., 2013. Surface and subsurface of the Metaponto
 1425 Coastal Plain (Gulf of Taranto-southern Italy): Present-day- vs LGM-landscape. *Geomorphology*
 1426 203, 115–131. <https://doi.org/10.1016/j.geomorph.2013.07.017>

1427 Truong, M.H., Nguyen, V.L., Ta, T.K.O., Takemura, J., 2011. Changes in late Pleistocene–Holocene
 1428 sedimentary facies of the Mekong River Delta and the influence of sedimentary environment on
 1429 geotechnical engineering properties. *Eng. Geol.* 122, 146–159.

1430 Urbano, T., Piacentini, T., Buccolini, M., 2017. Morphotectonics of the Pescara River basin (Central Italy).
 1431 *J. Maps* 13, 511–520. <https://doi.org/10.1080/17445647.2017.1338204>

1432 Vacchi, M., Marriner, N., Morhange, C., Spada, G., Fontana, A., Rovere, A., 2016. Earth-Science Reviews
 1433 Multiproxy assessment of Holocene relative sea-level changes in the western Mediterranean : Sea-
 1434 level variability and improvements in the definition of the isostatic signal. *Earth Sci. Rev.* 155,
 1435 172–197. <https://doi.org/10.1016/j.earscirev.2016.02.002>

1436 Van Wagoner, J.C., 1995. Sequence stratigraphy and marine to nonmarine facies architecture of foreland
 1437 basin strata, Book Cliffs, Utah, U.S.A, in: Van Wagoner, J.C., Bertram, G.T., (Eds.), Sequence
 1438 Stratigraphy of Foreland Basin Deposits: AAPG Memoir, 64, pp. 137-223.

1439 Van Wagoner, J.C., Mitchum, R.M., Campion, K.M., Rahmanian, V.D., 1990. Siliciclastic sequence
 1440 stratigraphy in well logs, cores, and outcrops: concepts for high-resolution correlation of time and
 1441 facies. AAPG Methods in Exploration 7.

1442 Van Wagoner, J.C., Posamentier, H.W., Mitchum, R.M., Vail, P.R., Sarg, J.F., Loutit, T.S., Hardenbol, J.,
 1443 1988. An Overview of the Fundamentals of Sequence Stratigraphy and Key Definitions, in: Wilgus,
 1444 C.K., Hastings, B.S., Kendall, C.G.C., H.W., P., Ross, C.A., Van Wagoner, J.C. (Eds.), Sea-Level
 1445 Changes: An Integrated Approach. SEPM Special Publication, 42, pp. 39–45.
 1446 <https://doi.org/10.2110/pec.88.01.0039>

1447 Walker, R.G., 1995. An Incised Valley in the Cardium Formation at Ricinus, Alberta: Reinterpretation as
 1448 an Estuary Fill., in: Plint, A.G. (Ed.), Sedimentary Facies Analysis. Wiley Online Library, pp. 47–
 1449 74. <https://doi.org/https://doi.org/10.1002/9781444304091.ch3>

1450 Wang, R., Colombero, L., Mountney, N.P., 2020. Quantitative analysis of the stratigraphic architecture of
 1451 incised-valley fills: A global comparison of Quaternary systems. Earth-Science Rev. 200, 102988.
 1452 <https://doi.org/10.1016/j.earscirev.2019.102988>

1453 Wang, R., Colombero, L., Mountney, N.P., 2019. Geological controls on the geometry of incised-valley
 1454 fills: Insights from a global dataset of late-Quaternary examples. Sedimentology 2134–2168.
 1455 <https://doi.org/10.1111/sed.12596>

1456 Wright, V.P., Marriott, S.B., 1993. The sequence stratigraphy of fluvial depositional systems: the role of
 1457 floodplain sediment storage. Sediment. Geol. 86, 203–210.

1458 Wu, C., Ye, G., Zhang, L., Bishop, D., Wang, J., 2015. Depositional environment and geotechnical
 1459 properties of Shanghai clay: a comparison with Ariake and Bangkok clays. Bull. Eng. Geol.
 1460 Environ. 74, 717–732.

1461 Yanbin, G., Tongyu, W., 2016. Discussion on the engineering geological stratification of the soft soil
 1462 deposited in deep-incised valley in Qiantang River of Hangzhou Bay. *J. Eng. Geol.* 24, 933–939.
 1463 <https://doi.org/10.13544/j.cnki.jeg.2016.s1.135>

1464 Yu, S.-Y., Berglund, B.E., Sandgren, P., Lambeck, K., 2007. Evidence for a rapid sea-level rise 7600 yr
 1465 ago. *Geology* 35, 891–894.

1466 Zaitlin, B.A., Dalrymple, R.W., Boyd, R., 1994. The stratigraphic organization of incised valley systems
 1467 associated with relative sea-level change, in: Dalrymple, R.W., Boyd, R., Zaitlin, B.A., (Eds.),
 1468 Incised-Valley Systems: Origin and Sedimentary Sequences. SEPM Special Publication 51, pp. 45-
 1469 60.

1470 Zecchin, M., Ceramicola, S., Lodolo, E., Casalbore, D., Chiocci, F.L., 2015. Episodic, rapid sea-level rises
 1471 on the central Mediterranean shelves after the Last Glacial Maximum: A review. *Mar. Geol.* 369,
 1472 212–223. <https://doi.org/10.1016/j.margeo.2015.09.002>

1473 Zeng, Z., Zhu, H., Mei, L., Du, J., Zeng, H., Xu, X., Dong, X., 2019. Multilevel source-to-sink (S2S)
 1474 subdivision and application of an ancient uplift system in South China Sea: Implications for further
 1475 hydrocarbon exploration. *J. Pet. Sci. Eng.* 181, 106220.

1476 Zhang, X., Li, X. long, Garzanti, E., Lin, C. ming, Deng, K., 2021. Sedimentary geochemistry response to
 1477 climate change on a millennial timescale in the Qiantang River incised-valley system, eastern
 1478 China. *Chem. Geol.* 586, 120587. <https://doi.org/10.1016/j.chemgeo.2021.120587>

1479 Zong, Y., Yim, W.-S., Yu, F., Huang, G., 2009. Late Quaternary environmental changes in the Pearl River
 1480 mouth region, China. *Quat. Int.* 206, 35–45.